Table 2 Electrophysiologic findings

Nerve	Responders	Nonresponders	*p* value*	Control, n = 121–191
All patients				
Median (R, n = 191; NR, n = 105)				
MCV, m/s	35.2 ± 13.2	39.8 ± 13.8	<0.01	57.8 ± 3.7
DL, ms	7.4 ± 5.3	6.4 ± 4.5	NS	3.4 ± 0.4
CMAP, mV	6.4 ± 4.6	5.3 ± 4.5	<0.05	10.7 ± 3.5
CB, %	45.5	27.5	<0.01	
Ulnar (R, n = 171; NR, n = 93)				
MCV, m/s	35.9 ± 12.7	39.0 ± 12.9	NS	58.6 ± 4.3
DL, ms	5.5 ± 5.0	5.0 ± 3.4	NS	2.7 ± 0.3
CMAP, mV	6.2 ± 4.2	4.8 ± 3.6	<0.005	8.4 ± 2.5
CB, %	50.9	41.3	NS	
Tibial (R, n = 168; NR, n = 81)				
MCV, m/s	33.7 ± 9.2	34.0 ± 9.4	NS	46.9 ± 3.5
DL, ms	7.5 ± 4.0	7.0 ± 3.0	NS	4.5 ± 0.8
CMAP, mV	5.7 ± 6.5	3.5 ± 5.9	<0.0001	10.9 ± 3.8
CB, %	40.5	35.6	NS	
Patients with similar duration (<12 mo)				
Median (R, n = 112; NR, n = 36)				
MCV, m/s	34.4 ± 12.5	40.5 ± 14.5	<0.05	57.8 ± 3.7
DL, ms	7.6 ± 4.8	8.3 ± 7.0	NS	3.4 ± 0.4
CMAP, mV	6.8 ± 4.6	4.2 ± 2.9	<0.01	10.7 ± 3.5
CB, %	33.0	20.0	<0.05	
Ulnar (R, n = 101; NR, n = 33)				
MCV, m/s	35.6 ± 11.4	37.6 ± 15.3	NS	58.6 ± 4.3
DL, ms	5.5 ± 3.6	5.5 ± 2.5	NS	2.7 ± 0.3
CMAP, mV	5.9 ± 4.2	4.0 ± 3.6	<0.05	8.4 ± 2.5
CB, %	50.8	44.4	NS	
Tibial (R, n = 102; NR, n = 25)				
MCV, m/s	33.5 ± 9.0	33.4 ± 8.5	NS	46.9 ± 3.5
DL, ms	7.9 ± 4.0	8.0 ± 3.1	NS	4.5 ± 0.8
CMAP, mV	5.2 ± 5.5	1.9 ± 2.8	<0.0005	10.9 ± 3.8
CB, %	48.8	44.4	NS	

* *p* value indicates a significant difference between responders and nonresponders.

R = responder; NR = nonresponder; MCV = motor nerve conduction velocity; DL = distal latency; CMAP = compound muscle action potential; CB = conduction block.

StatView software for Macintosh (version 4.5; Abacus Concepts, Berkeley, CA).

Results. *Clinical findings.* Efficacy of IVIg therapy was 63.8% (table 1 and table E-1 on the *Neurology* Web site at www.neurology.org). The rate of patients whose symptomatic exacerbation stopped 3 months after onset was higher in responders than in nonresponders. Responders showed significantly more severe weakness of the upper and proximal lower limbs, whereas nonresponders showed more marked muscle atrophy in the upper and lower limbs. As the disease duration from onset to IVIg differed significantly between responders and nonresponders in the patients as a whole, we additionally compared the subgroups of responders and nonresponders with disease duration of <12 months, eliminating significant differences about the disease duration.

Efficacy of IVIg in the patients with similar duration was 79.9%. The rate of patients whose symptomatic exacerbation stopped 3 months after onset was still higher in responders. Muscle atrophy of each limb was significantly more prominent in nonresponders, as was true for the patients as a whole.

Electrophysiologic findings. Mean CMAP was significantly more reduced in the median, ulnar, and tibial nerves in nonresponders (table 2 and table E-2). Frequency of conduction block showed a tendency to be more pro-

Table 3 *Electrophysiologic findings before and after IVIg therapy*

Nerve	Pre IVIg	Post IVIg	*p* value*
Responders, n = 71			
Median			
MCV, m/s	32.4 ± 13.2	35.3 ± 12.4	<0.05
DL, ms	6.6 ± 4.0	6.7 ± 4.7	NS
CMAP, mV	5.6 ± 4.1	6.7 ± 4.6	NS
CB, %	45.7	38.9	<0.05
Ulnar			
MCV, m/s	33.5 ± 11.3	36.7 ± 11.1	<0.01
DL, ms	5.3 ± 2.8	4.8 ± 2.7	NS
CMAP, mV	5.3 ± 3.1	5.8 ± 3.3	NS
CB, %	42.2	35.7	<0.05
Tibial			
MCV, m/s	31.5 ± 8.3	33.3 ± 10.4	<0.05
DL, ms	7.1 ± 3.1	7.1 ± 4.3	NS
CMAP, mV	3.5 ± 3.2	4.4 ± 4.3	NS
CB, %	44.8	27.6	<0.01
Nonresponders, n = 51			
Median			
MCV, m/s	38.5 ± 13.6	39.1 ± 13.7	NS
DL, ms	7.3 ± 4.1	7.7 ± 4.8	NS
CMAP, mV	5.9 ± 5.0	5.6 ± 4.7	NS
CB, %	32.7	23.5	NS
Ulnar			
MCV, m/s	36.0 ± 14.4	34.0 ± 12.5	NS
DL, ms	5.6 ± 2.4	5.5 ± 2.1	NS
CMAP, mV	4.4 ± 3.3	4.2 ± 3.9	NS
CB, %	40.9	35.0	NS
Tibial			
MCV, m/s	30.5 ± 9.7	32.7 ± 10.3	NS
DL, ms	7.8 ± 3.6	7.5 ± 3.7	NS
CMAP, mV	3.2 ± 4.1	4.1 ± 4.9	NS
CB, %	46.5	46.2	NS

* *p* value indicates a significant difference between responders and nonresponders.

IVIg = IV immunoglobulin; MCV = motor nerve conduction velocity; DL = distal latency; CMAP = compound muscle action potential; CB = conduction block.

nounced in responders. In the patients with similar durations, electrophysiologic findings also resembled those for patients as a whole. Mean CMAP was significantly more reduced in nonresponders, and conduction block tended to be more frequent in responders.

Electrophysiologic findings before and after IVIg therapy. We assessed electrophysiologic changes before and after IVIg (table 3). Mean MCV in the median, ulnar, and tibial nerves in responders improved significantly after IVIg, whereas mean CMAP in the same nerves did not. In contrast, both mean MCV and mean CMAP in nonresponders did not improve significantly. Conduction block became less frequent after IVIg in responders.

Discussion. One cardinal finding was that features related to axonal dysfunction were a major contribution to unresponsiveness to IVIg therapy in CIDP. More severe CMAP amplitude reduction and more severe muscle atrophy were seen in nonresponders than in responders. MCV and distal latency were essentially similar between responder and nonresponder groups, but conduction block was more frequent in responders, suggesting that IVIg responsiveness was linked to demyelinating as opposed to axonal features.

In the previous reports, nonresponsiveness has been suggested to be caused by the longer interval from symptom onset to initiation of IVIg therapy.[9] One possible explanation for the longer duration effect might be that secondary axonal degeneration could follow segmental demyelination in patients with long symptomatic intervals prior to effective therapy, as suggested in primary demyelination. Accordingly, we compared features between subgroups of responders and nonresponders who had similar disease duration from onset, obtaining similar results that axonal dysfunction remained the major determinant of IVIg unresponsiveness. These observations suggest that whereas symptom duration before treatment was one determinant of IVIg ineffectiveness in CIDP, duration-independent axonal dysfunction was another. According to recent reports, demyelination-independent primary axonal damage has been suggested to occur in a subgroup of CIDP cases, termed the axonal variant of CIDP. These findings support our view that duration-independent axonal features can exist in CIDP and thus contribute to treatment failure.[5,9,10]

In addition, electrophysiologic impairment is more reversible in responders than in nonresponders, and demyelinating features are effectively improved by IVIg. Axonal features, less reversible with IVIg, were more prominent in nonresponders. Nonresponders also did not show any improvement in MCV, CMAP, or frequency of conduction block. The current results suggest that the pathologic dysfunction of peripheral nerves differs between responders and nonresponders.

References

1. Research criteria for diagnosis of chronic inflammatory demyelinating polyneuropathy (CIDP). Report from an Ad Hoc Subcommittee of the American Academy of Neurology AIDS Task Force. Neurology 1991;41:617–618.
2. Choudhary PP, Hughes RA. Long-term treatment of chronic inflammatory demyelinating polyradiculoneuropathy with plasma exchange or intravenous immunoglobulin. Q J Med 1995;88:493–502.
3. van Doorn PA, Brand A, Strengers PF, Meulstee J, Vermeulen M. High-dose intravenous immunoglobulin treatment in chronic inflammatory demyelinating polyneuropathy: a double-blind, placebo-controlled, crossover study. Neurology 1990;40:209–212.
4. van Doorn PA, Vermeulen M, Brand A, Mulder PG, Busch HF. Intravenous immunoglobulin treatment in patients with chronic inflammatory demyelinating polyneuropathy. Clinical and laboratory characteristics associated with improvement. Arch Neurol 1991;48:217–220.

5. Boukhris S, Magy L, Kabore R, et al. Atypical electrophysiological findings in chronic inflammatory demyelinating polyneuropathy (CIDP)—diagnosis confirmed by nerve biopsy. Neurophysiol Clin 2004;34:71–79.
6. Koike H, Iijima M, Sugiura M, et al. Alcoholic neuropathy is clinicopathologically distinct from thiamine-deficiency neuropathy. Ann Neurol 2003;54:19–29.
7. Merkies IS, Schmitz PI, van der Meche FG, Samijn JP, van Doorn PA. Clinimetric evaluation of a new overall disability scale in immune-mediated polyneuropathies. J Neurol Neurosurg Psychiatry 2002;72:596–601.
8. The Dutch TIA Trial: protective effects of low-dose aspirin and atenolol in patients with transient ischemic attacks or nondisabling stroke. Stroke 1988;19:512–517.
9. Hahn AF, Bolton CF, Zochodne D, Feasby TE. Intravenous immunoglobulin treatment in chronic inflammatory demyelinating polyneuropathy. A double-blind, placebo-controlled, cross-over study. Brain 1996; 119:1067–1077.
10. Sahenk Z. Abnormal Schwann cell-axon interactions in CMT neuropathies. The effects of mutant Schwann cells on the axonal cytoskeleton and regeneration-associated myelination. Ann NY Acad Sci 1999;883: 415–426.

American Journal of Pathology, Vol. 166, No. 2, February 2005

Neurobiology

Accumulation of Filamentous Tau in the Cerebral Cortex of Human Tau R406W Transgenic Mice

Masaki Ikeda,* Mikio Shoji,† Toshitaka Kawarai,‡ Takeshi Kawarabayashi,§ Etsuro Matsubara,§ Tetsuro Murakami,§ Atsushi Sasaki,¶ Yasushi Tomidokoro,* Yasushi Ikarashi, Hisashi Kuribara,** Koichi Ishiguro,†† Masato Hasegawa,‡‡ Shu-Hui Yen,§§ M. Azhar Chishti,‡ Yasuo Harigaya,¶¶ Koji Abe,§ Koichi Okamoto,* Peter St. George-Hyslop,‡ and David Westaway‡

From the Department of Neurology, Department of Human Pathology,¶ Gunma University Graduate School of Medicine, Gunma, Japan; the Department of Neurology,§ Neuroscience, Biophysiological Science, Okayama University Graduate School of Medicine and Dentistry, Okayama, Japan; the Centre for Research in Neurodegenerative Diseases,‡ Departments of Medicine (Neurology) and Laboratory Medicine and Pathobiology, University of Toronto, University Health Network, Toronto, Ontario, Canada; the Department of Neurology,¶¶ Maebashi Red Cross Hospital, Gunma, Japan; the Mitsubishi Kagaku Institute of Life Sciences,†† Tokyo, Japan; the Department of Molecular Neurobiology,‡‡ Tokyo Institute of Psychiatry, Tokyo, Japan; R&D Division, Tsumura & Co., Ltd., Ibaraki, Japan; the Laboratory of Development,** Wakamyaku Medical Institute, Ltd., Gunma, Japan; and the Mayo Clinic Jacksonville,§§ Jacksonville, Florida*

Missense mutations of the *tau* gene cause autosomal dominant frontotemporal dementia and parkinsonism linked to chromosome 17 (FTDP-17), an illness characterized by progressive personality changes, dementia, and parkinsonism. There is prominent frontotemporal lobe atrophy of the brain accompanied by abundant tau accumulation with neurofibrillary tangles and neuronal cell loss. Using a hamster prion protein gene expression vector, we generated several independent lines of transgenic (Tg) mice expressing the longest form of the human four-repeat *tau* with the R406W mutation associated with FTDP-17. The TgTauR406W 21807 line showed tau accumulation beginning in the hippocampus and amygdala at 6 months of age, which subsequently spread to the cortices and subcortical areas. The accumulated tau was phosphorylated, ubiquitinated, conformationally changed, argyrophilic, and sarcosyl-insoluble. Activation of GSK-3 and astrocytic induction of mouse tau were observed. Astrogliosis and microgliosis correlated with prominent tau accumulation. Electron microscopic examination revealed the presence of straight filaments. Behavioral tests showed motor disturbances and progressive acquired memory loss between 10 to 12 months of age. These findings suggested that TgTauR406W mice would be a useful model in the study of frontotemporal dementia and other tauopathies such as Alzheimer's disease (AD). ***(Am J Pathol 2005, 166:521–531)***

Frontotemporal dementia and parkinsonism linked to chromosome 17 (FTDP-17) is a familial neurodegenerative disease characterized by autosomal dominant inheritance, personality change, progressive dementia, and parkinsonism. Extensive tau accumulation with neurofibrillary tangles (NFT) and loss of neurons are characteristic pathological changes and are associated with frontotemporal lobe atrophy.[1] Following the initial discovery of missense mutations in the *tau* gene,[2–4] numerous exonic and intronic mutations have been reported.[5] The majority of mutations are clustered within or close to the microtubule (MT)-binding domains, or in the 5 -splice site of exon 10.[5] Most of the exonic mutations lead to tau proteins with a decreased ability to promote MT assembly and an increase in self-aggregation.[6] Some of the exonic, and all of the intronic, mutations cause an increase in the level of four-repeat tau.[3,4] An increase in

Supported by Scientific Research on Priority Areas (C)-Advanced Brain Science Project-(M.I. no. 15016018) and Grants-in-Aid for Scientific Research (C) (2) (M.I. no. 15590879), Grants-in-Aid for Primary Amyloidosis Research Committee (M.S.), and by Grants-in-Aid for Scientific Research (B) (M.S. no. 16390251) and Scientific Research on Priority Areas (C)-Advanced Brain Science Project-(M.S.) from the Ministry of Education, Culture, Sports, Science and Technology, Japan, the Canadian Institutes for Health Research, the Howard Hughes Medical Institute, the Canadian Genetic Diseases Network, and the Alzheimer Society of Ontario (P.S.G.-H.).

Accepted for publication October 21, 2004.

Address correspondence to Masaki Ikeda, M.D., Ph.D., Department of Neurology, Gunma University Graduate School of Medicine, 3–39-22 Showa-machi, Maebashi, Gunma, 371-8511, Japan, E-mail: mikeda@med.gunma-u.ac.jp.

four-repeat tau is hypothesized to promote tau self-aggregation and decrease MT assembly.[7] These gain-of-function effects have been suggested to cause tau accumulation leading to NFT formation and neuronal cell death.

Several neurodegenerative diseases that display tau accumulation, such as Alzheimer's disease, frontotemporal dementia, Pick's disease, progressive supranuclear palsy, and corticobasal degeneration are now classified as tauopathies.[8] It is therefore important to clarify the mechanism by which mutant tau accumulates and leads to NFT formation and to determine whether or not there is a single common pathological pathway of tauopathies. Although pedigrees segregating the *tau* R406W mutation have a variety of clinical and pathological characteristics, consistent pathological features include frontotemporal atrophy, abundant tau accumulation, and neurofibrillary tangles containing both paired helical filaments and straight filaments.[9–11] The *tau* R406W mutation has far a weaker effect on MT assembly-promoting activity than that of *tau* P301L and *tau* V337M mutations,[6] and stable or transient transfection of tau R406W in non-neuronal cell lines showed that tau R406W was less phosphorylated than wild-type tau.[12] While the sarcosyl-soluble tau R406W was less phosphorylated than sarcosyl-soluble wild-type tau, sarcosyl-insoluble tau R406W was as highly phosphorylated as the insoluble wild-type tau.[13] These results suggested unique molecular effects of tau R406W on NFT formation. For this reason, we generated transgenic (Tg) mice expressing tau R406W (TgTauR406W). These mice were then followed using behavioral, neuropathological, and neurochemical methods. While the majority of these mice did not develop an overt behavioral or neuropathological phenotype, a small proportion of these mice (20%) developed a behavioral, neuropathological, and neurochemical phenotype that displayed several features reminiscent of human tauopathies. The cause of this variation in expressivity/penetrance is being explored and remains unknown (possibly the effects of genetic background modifiers although environmental effects cannot yet be excluded). Nevertheless, in its most highly expressed form, the TgTauR406W mice developed an illness characterized by extensive accumulation of tau and subsequent alterations in the neocortex, hippocampus, and amygdala associated with motor and memory disturbances.

Materials and Methods

Transgene Construction, Generation of Transgenic Mice, and Analysis of RT-PCR

The longest isoform of wild-type human four-repeat *tau* cDNA containing a eukaryotic Kozak initiation sequence (GCCGCCACC)[14,15] upstream of the start codon was ligated into the *Sal*I restriction site of the *cos.tet* expression vector containing the Syrian hamster prion protein promoter gene,[16] packaged *in vitro* and plated on *E. coli* DH1 to obtain a bacterial stock containing the recombinant cosmid clone. To generate the *tau* R406W mutation, wild-type human four-repeat *tau* cDNA was mutated by an oligonucleotide-mediated method with a proofreading DNA polymerase ("Quick change", Stratagene, La Jolla, CA). Following confirmation of the site-directed mutagenesis by direct sequencing, the mutated *tau* R406W cDNA was reintroduced into the *cos.tet* expression vector. The transgenes were purified and microinjected into fertilized oocytes of FVB/N mice as previously described.[17,18] Positive founders were subsequently bred with FVB wild-type mice and offspring were genotyped using a human *tau* cDNA fragment radiolabeled by the random-primer method.

To analyze gene expression of human *tau*, RT-PCR was performed using 2 l of mRNA isolated using the QuickPrep Micro mRNA purification kit (Amersham Biosciences, UK) from brains of Tg mice (21807) and non-Tg mice brains at 6 and 10 months old (*n* 3, respectively) in the reaction tube of Ready-To-Go RT-PCR Beads (Amersham Biosciences, UK) with PCR primers sets as follows: mouse *tau* exon 9F (5 -CACCAAAATCCG-GAGAACGA-3) and mouse exon 11R (5 -CTTTGCT-CAGGTCCACCGGC-3): human *tau* exon 9F (5 -CTC-CAAAATCAGGGGATCGC-3) and human *tau* exon 11R (5 -CCTTGCTCAGGTCAACTGGT-3). PCR conditions included 30 cycles of 94°C for 30 seconds, 62°C for 30 seconds, 72°C for 45 seconds with a final 72°C extension phase for 10 minutes, as in a previous report.[19] For semi-quantification, RT-PCR of -actin was performed as internal control.[20] Ten l of PCR products were analyzed by 2.5% agarose gel elecrophoresis. The intensity of ethidium-stained bands was analyzed by Scion Image (Scion Corporation, USA).

Transgenic founders were used to create Tg mice lines bearing the *tau* R406W mutation: TgTauR406W 21807, TgTauR406W 21783, and TgTauR406W 21768. Twenty-one positive Tg progenies, 16 F1 Tg and 98 F2 Tg were analyzed. The TgTauR406W 21807 line (*n* 11) was used for the rotarod and passive avoidance tests. All animal experiments were performed according to guidelines established in the "Guide for the Care and Use of Laboratory Animals."

Antibodies

The following antibodies were used: two human tau-specific antibodies, anti-tau154 (1:200; antibody to synthetic amino acids of 154–168 of human tau 441), E1 (1:1000)[21] and two human and mouse tau antibodies, PHF-1 (1:100, kindly provided by Dr. P. Davies, Albert Einstein College of Medicine),[22] and anti-tau-C against C-terminal tau (1:200, 422–438 amino acid of human tau 441),[23] a conformation-dependent tau antibody Alz-50 (1:100, kindly provided by Dr. P Davies);[24] an anti-glial fibrillary acidic protein antibody (GFAP, 1:20,000, DAKO, Denmark), an anti-microglia antibody (F4/80, 1:20, BMA Biomedicals, Switzerland), an anti-ubiquitin antibody (1:500, kindly provided by Dr. D. Dickson, Mayo Clinic Jacksonville); phosphorylation-site specific tau antibodies: anti-PS199 (phosphorylated serine 199, 1:500),[25,26] CP13 (phosphorylated at serine 202, 1:100, kindly provided by

Dr. P. Davies),[27] AT8 (phosphorylated serine 202/threonine 205, 1:2000),[28] anti-PT205 (phosphorylated threonine 205, 1:100),[26] anti-PT231/PS235 (phosphorylated threonine 231/serine 235, 1:500),[26] anti-PS396 (phosphorylated serine 396, 1:500)[26] and anti-PS413 (phosphorylated serine 413, 1:100)[26]; antibodies against kinase for tau phosphorylation: anti-glycogen synthase kinase-3 (anti-GSK-3 , 1:50),[25,26] anti-GSK-3 (1:100),[25,26] anti-PY216 (anti-activated GSK-3 , 1:250),[25,26,29] anti-PS9 (anti-inactive GSK-3 , 1:25),[25,26] anti-Cdk5 antibody (anti-cyclin-dependent kinase 5, 1:100)[25,26] and anti-MAPK (anti-mitogen-activated protein kinase, 1:250).[25,26]

Tissue Preparation and Staining

After mice were sacrificed under ether anesthesia, brains were removed and cut sagittally at the midline. One hemisphere was fixed in 4% paraformaldehyde with 0.1 mol/L phosphate buffer (PB, pH 7.6) for 1 week and embedded in paraffin. Five m-thick sections were prepared for staining. Sections were immersed in 0.5% periodic acid and treated with 99% formic acid for 3 minutes for tau immunostaining. After blocking with 5% normal goat serum in 50 mmol/L phosphate-buffered saline (PBS) containing 0.05% Tween 20 and 4% Block Ace (Snow Brand, Japan), sections were incubated for 6 hours with the primary antibodies. The specific labeling was visualized using a Vectastain Elite ABC kit (Vector Labs, Burlingame, CA). These tissue sections were counterstained with hematoxylin. Conventional Gallyas-Braak silver staining for NFT and Nissl staining for neuronal cell counts were performed. We adopted the terminology defined based on an atlas of the mouse brain.[30] The number of neurons/mm^2 was counted in three Nissl-stained 5-mm sections from the piriform cortex and amygdala of 11 Tg mice, including no. 8859 and no. 9731, and 11 age-matched 10-month-old non-Tg mice.

Electron Microscopic Study

The brain tissues were immersed in a fixative solution (2.5% glutaraldehyde, 0.1 mol/L phosphate buffer, pH 7.4) for 4 hours and washed several times in 0.1 mol/L PB containing 7% sucrose. Blocks were then post-fixed in 2% osmium tetroxide, dehydrated in ethanol and propylene oxide, and embedded in Quetol 812 (Nisshin EM, Japan). Ultra-thin sections were stained with uranyl acetate and lead acetate before observation with an electron microscope.

For immuno-electron microscopic study, PBS-washed pellets, after sarcosyl extraction of Tg mice brains, were applied to carbon-coated 400 mesh EM grids (VECO, Holland). The samples were incubated with an anti-tau154 antibody at room temperature for 3 hours. Each specimen was washed with PBS and incubated with 12-nm colloidal gold conjugated anti-rabbit IgG (Jackson Immunoresearch Labs, PA) at room temperature for 1 hour, then examined by electron microscopy (EM).

Western Blot Analysis

Half of the brains from Tg or non-Tg mice at 5 and 13 months of age were weighed and homogenized using a Teflon-homogenizer in nine volumes of Tris-saline buffer (TS) with protease inhibitors (TS inhibitors: 50 mmol/L Tris-HCl and 150 mmol/L NaCl, pH 7.6, 0.5 mmol/L DIFP, 0.5 mmol/L PMSF, 1 g/ml TLCK, 1 g/ml antipain, 1 g/ml leupeptin, 0.1 g/ml pepstatin, 1 mmol/L EGTA). The homogenate was centrifuged at 55,000 rpm for 60 minutes at 4°C and the supernatant was analyzed as the TS-soluble fraction. Then, the pellets were homogenized again in four volumes of 1% sarcosyl in TS inhibitors, incubated on ice for 30 minutes, and centrifuged at 55,000 rpm for 60 minutes at 4°C. The supernatant and pellet were analyzed as sarcosyl-soluble or sarcosyl-insoluble fractions, respectively. Each 2 l of sample was boiled at 70°C in four volumes of sodium dodecylsulfate (SDS) sample buffer and separated on 4 to 12% NuPAGE Bis-Tris Gel (Invitrogen Corp., Carlsbad, CA). The signal intensity was detected using the ECL-Plus system (Amersham Bioscience Corp., NJ) and a luminoimage analyzer (LAS 1000-Mini, Fuji Film, Tokyo).

Rotarod Test

Tg mice (n 11) and age-matched non-Tg control mice (n 11) at 10 and 12 months old were assessed for how long they could stay on a rotating rod treadmill apparatus (Ugo Basile, Biological Research Apparatus, Milan, Italy). Mice were placed on the rod rotating at a speed of 16 rpm for 30 seconds, and the time they stayed on the rotating rod was measured. The trial was performed three times and then repeated three additional times after 10 minutes of rest for every mouse. Statistical analysis was conducted by the Mann-Whitney test.

Step-Through Passive Avoidance Test

Tg mice (n 11) and age-matched non-Tg control mice (n 11) at 10 months of age were examined. The apparatus (AP model, O'Hara Co., Tokyo, Japan) for the step-through passive avoidance test consisted of two compartments; one was illuminated [light at the top of the compartment (27 watt, 3000 lux)] and the other was a dark compartment. After the mouse was placed in the illuminated safe compartment, the compartment was lit, and the mouse stepped through an open guillotine door into the dark compartment. The time spent in the illuminated compartment was defined as the latency time. Three seconds after the mouse entered the dark compartment, a foot-shock (0.3 mA, 50 V, 50 Hz AC, for 3 seconds) was given. The retention of avoidance memory trials was carried out once a week for 9 weeks after 5 days of serial acquisition trials. The retention latency time was measured for up to 300 seconds without delivering a foot-shock.[31,32] Statistical analysis was performed by a two-way repeated measure analysis of variance (SPSS Version 11).

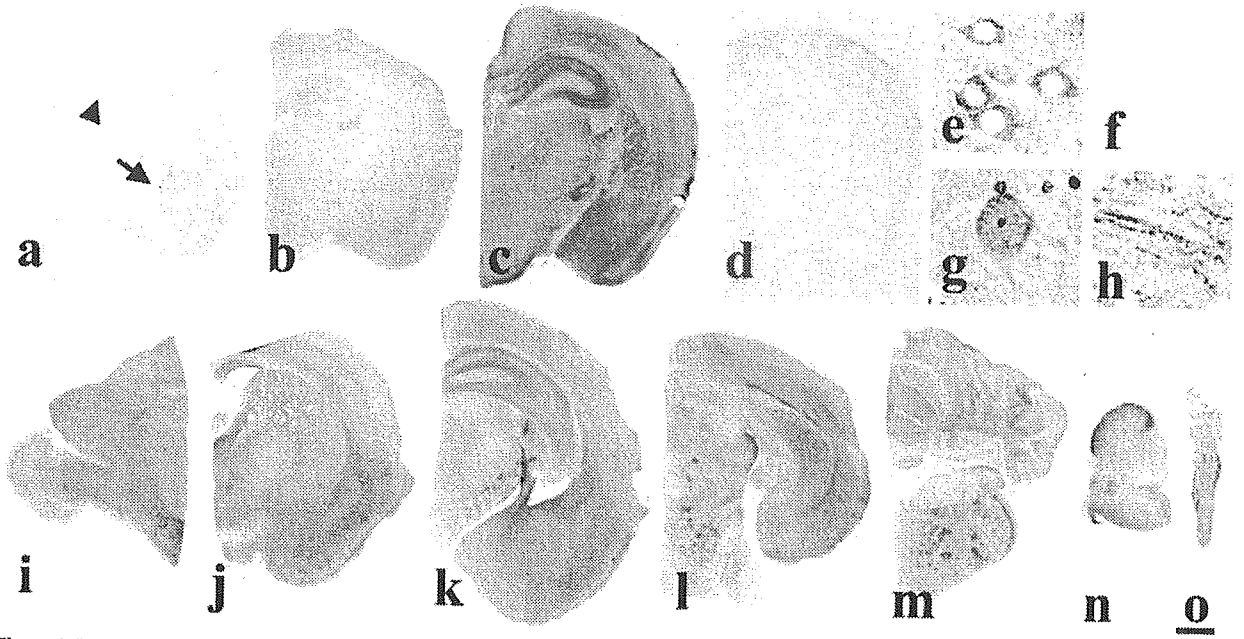

Figure 1. Progress and distribution of human tau accumulation. In 6-month-old TgTauR406W 21807 mice, human tau is detected in the hippocampus and the amygdala (**arrowhead ▲**, hippocampus; **arrow →**, amygdala) (**a**). Accumulation of human tau has spread to the neocortex, which corresponded to the neocortex in mouse pathology, and caudate putamen, in addition to the hippocampus at 8 months of age (**b**). In 14-month-old TgTauR406W 21807 mice, human tau is widely accumulated in the neocortex and subcortical regions (**c**). No human tau accumulation is found in age-matched non-Tg mice brains (**d** and **f**). Tau accumulated in the cell bodies (**e**, neocortex; **g**, anterior horn cells) and processes (**h**) of neuronal cells. Accumulation of human tau is prominent in the neocortex and the piriform cortex (**i** to **k**), hippocampus (**k** and **l**), amygdala (**l**), cerebellum (**m**), and spinal cord (**n** and **o**) at 10 months of age. Anti-tau154 antibody staining. **Bar**, 0.5 mm (**a–d** and **i–o**); 12.5 m (**e–h**).

Results

Progression and Distribution of Tau Accumulation in Brains of Tg Mice

At 3 months of age (*n* 5), there was no detectable accumulation of human tau by immunocytochemistry. At 6 months of age (*n* 5), tau 154 labeled some neurons and processes in the dentate gyrus of the hippocampus (Figure 1a, arrowhead) and neurons in the amygdala (Figure 1a, arrow). At 8 months of age (*n* 5), tau deposition was observed in the cell bodies and processes of neurons of the neocortex, hippocampus, and amygdala (Figure 1b). At 14 months old (*n* 4), accumulation of tau protein progressively extended to the caudate putamen, white matter, and cerebellar cortex (Figure 1c). This tau immunoreactivity was enhanced by formic acid pretreatment. Human tau was not detected in the brains of non-Tg control mice at 14 months of age (Figure 1d).

Accumulation of human tau was intensely observed in the neocortex and the piriform cortex, amygdala, and hippocampus in 10-month-old Tg mice brains (*n* 13) (Figure 1, i to k). In the neocortex, accumulation of tau was prominent in layer II and IV-VI (Figure 1k). Moderate accumulation of tau was observed in the entorhinal cortex, caudate putamen, anterior and posterior horn of the spinal cord, brainstem and cortex of the cerebellum (Figure 1, l to o). The staining of tau in the olfactory bulb, thalamus, and hypothalamus was weak (Figure 1, i to l). Tau was also observed in subcortical areas, such as the corpus callosum, internal capsule, white matter of the cerebellum, and white matter of the spinal cord. No atrophy was observed in skeletal muscles. The accumulated tau localized predominantly in the cell bodies and processes of the neocortical neurons (Figure 1e). Granular dot-like stainings were frequently observed all around the neurons (Figure 1e). No human tau was observed in non-Tg control mice (Figure 1f). Tau accumulated in the cell bodies and dendrites of neurons in the anterior horn of the spinal cord (Figure 1g) and in neuronal processes in the neocortex (Figure 1h).

Reactive Changes following Tau Accumulation in Tg Mice Brains

In 10-month-old Tg mice, GFAP immunostaining demonstrated marked astrogliosis in the neocortex, amygdala (Figure 2a, arrow), and hippocampus (Figure 2a, arrowhead) compared with non-Tg mice (Figure 2b). Numerous large GFAP-positive bizarre astrocytes were prominent in the amygdala and hippocampus (Figure 2c). These reactive astrocytes were not detected in non-Tg control mice (Figure 2d), and they were not stained with anti-tau 154 (Figure 2e, arrow). However, anti-tau-C antibody labeled these astrocytes (Figure 2f, arrow), suggesting that intrinsic murine tau was induced in these glial cells. F4/80 staining showed more prominent microgliosis in the neocortex, amygdala and hippocampus of Tg mice (Figure 2g) compared with non-Tg control mice (Figure 2h). In a TgTauR406W 21807 (no. 8859) mouse

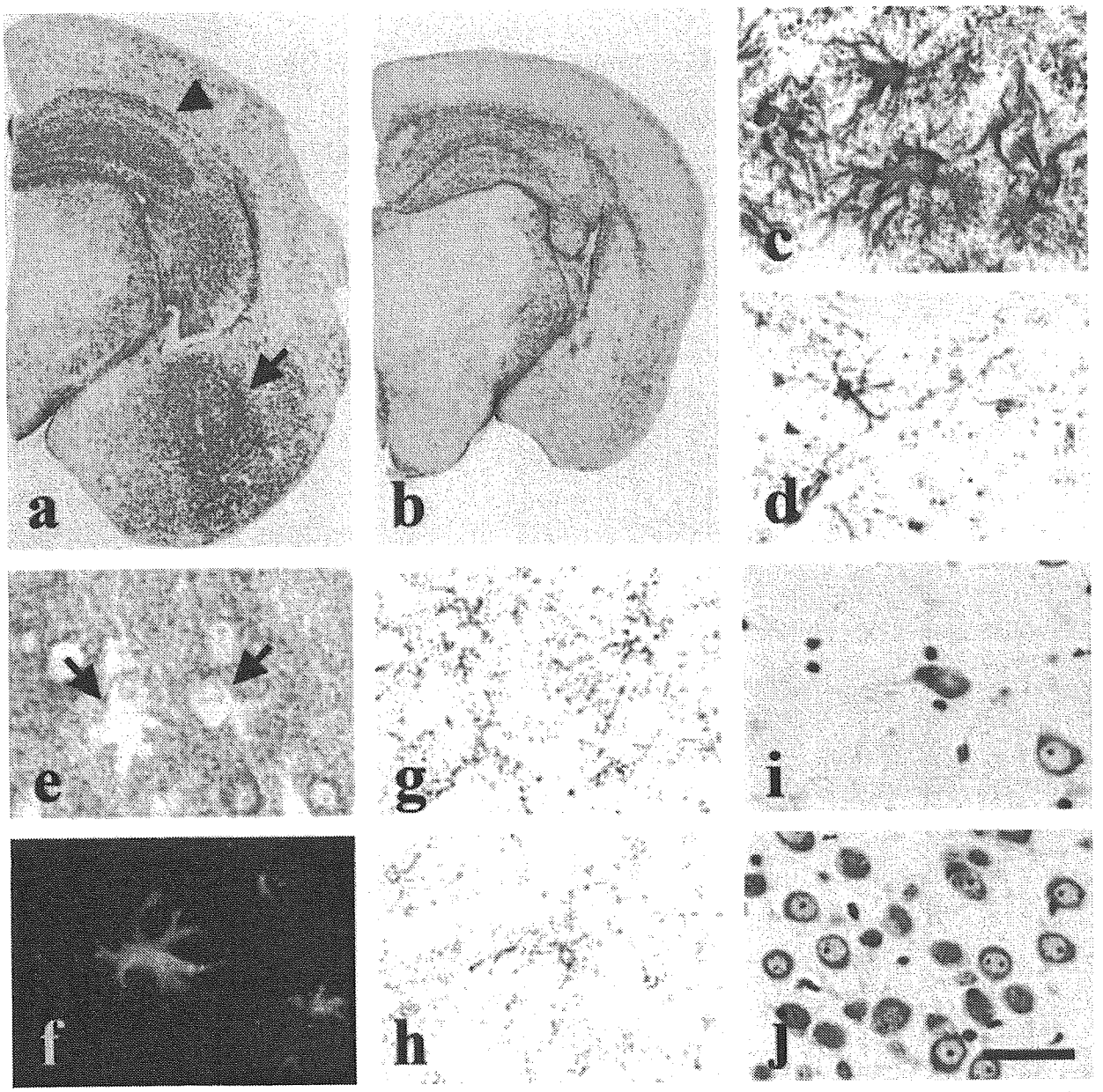

Figure 2. Reactive changes. In TgTauR406W 21807 mice, extensive astrogliosis is detected in the hippocampus, amygdala and neocortex (**arrowhead ▲**, hippocampus; **arrow →**, amygdala) (**a**) compared with non-Tg controls (**b**). At high magnification of the amygdala (**a**), numerous large bizarre astrocytes are shown in the Tg mice (**c**), but not in the non-Tg mice brains (**d**). In the bizzare astrocytes, human tau R406W is not observed (→) (**e**). However, these astrocytes express endogenous mouse tau (→) (**f**). Microgliosis is more prominent in the Tg mice brains (**g**) compared with the brain of a control mouse (**h**). In the amygdala of 21807 mice, the number of neuronal cells is decreased (**i**) compared with the non-Tg mice brains (**j**). **Bar**, 1 mm (**a** and **b**); 50 m (**c–j**).

that presented with rapidly progressive and severe akinesia, and which had the most severe pathological alterations, there was a subjective impression that number of neuronal cells was decreased in the amygdala (Figure 2i) and the piriform cortex in comparison with those of non-Tg control mice (Figure 2j).

Although formal stereological cell counts have not been performed, there did not appear to be any massive and consistent patterns of neuronal cell loss. A subset of Tg mice appeared to have reduced neuronal cell number that did not reach significance when overall quantification of neurons was performed. However, no A amyloid deposition was induced in the brains of Tg mice (data not shown).

Phosphorylation and Ubiquitination of Accumulated Tau in Tg Mice Brains

To investigate whether the accumulated tau was phosphorylated and ubiquitinated, we analyzed 10-month-old Tg mice brains by immunocytochemistry using several antibodies, which identify the PHF of Alzheimer's disease.[33] The accumulated human tau R406W in the cell

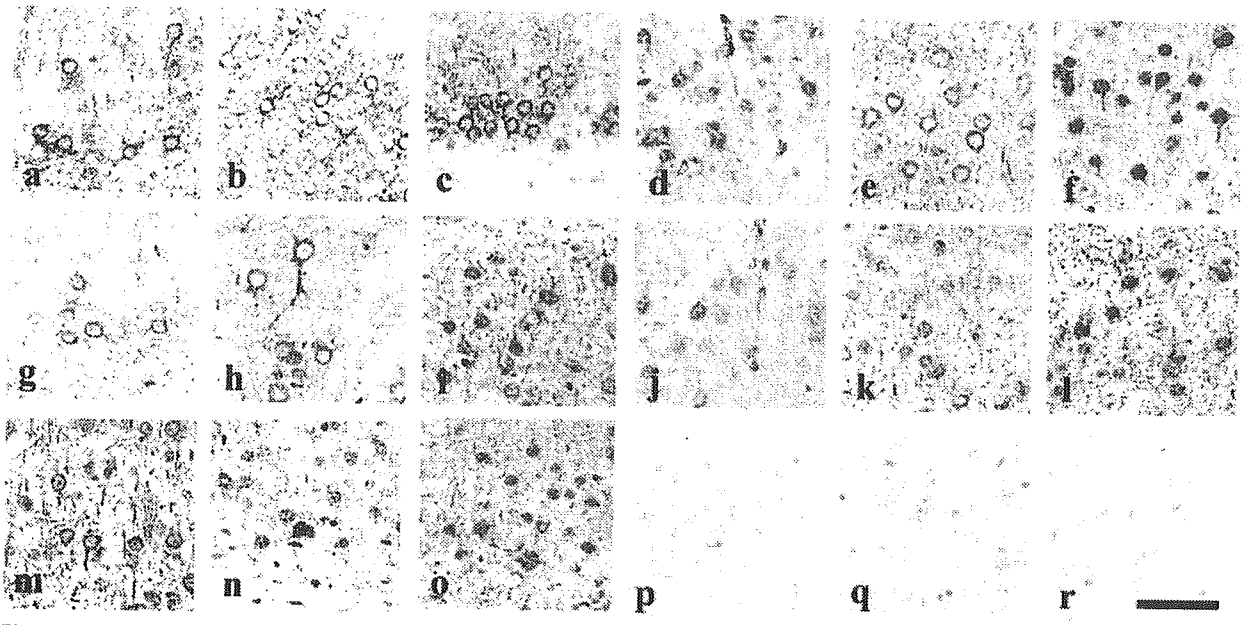

Figure 3. Phosphorylation of accumulated tau. In the Tg mice brains, anti-tau154 antibody-labeled tau accumulations are seen in neurons and processes and as small round dot-like stains (**a**). These structures are labeled by both E1 (**b**) and PHF-1 antibodies (**c**). Antibody CP13 (**d**), Alz-50 (**e**) labeled neuronal cell bodies and dendrites. Anti-ubiquitin antibody stained neuronal cell bodies and dendrites (**f**). Phosphorylated tau antibodies PS199, AT8 and PT205, PT231/PS235, PS396, PS413 labeled neuronal cell bodies and dendrites (**g–l**). Anti-GSK-3 antibody labeled cell bodies of neurons (**m**). Anti-PY216 antibody against activated GSK-3 immunostained cell bodies of neurons (**n**), which are also stained by Cdk5 (**o**). Neither anti-PS9 against non-activated GSK-3 , anti-GSK-3 , nor anti-MAPK labeled these neurons (**p** to **r**). **Bar**, 50 m.

bodies and neuronal processes of the piriform cortices was labeled by the human tau-specific antibodies anti-tau 154 (Figure 3a) and E1 (Figure 3b). PHF-1 (Figure 3c) and antibody CP13 (Figure 3d) labeled cell bodies mainly. Alz-50 (Figure 3e) similarly immunostained neuronal cell bodies and processes. The anti-ubiquitin antibody (Figure 3f) labeled cell bodies with nuclear staining and processes. Phosphorylation site-specific tau antibodies, PS199, AT8(Ser202/Thr205), PT205, PT231/PS235, PS396, and PS413 similarly labeled neuronal cell bodies and processes (Figure 3, g to l). These findings suggested that the accumulated tau was phosphorylated and ubiquitinated as is seen in PHF tau in Alzheimer's disease. To investigate what kind of kinase was activated in forming phosphorylated tau in Tg mice, kinases associated with PHF tau were examined. Anti-GSK-3 labeled the axons, dendrites, and cell bodies of neuronal cells in neocortices and the hippocampus area (Figure 3m). Anti-PY216 labeled the cell bodies of neuronal cells (Figure 3n). The anti-Cdk5 antibody labeled the processes and cell bodies of neuronal cells (Figure 3o), while non-Tg mice did not show any such immunostaining (not shown). Anti-PS9, anti-GSK-3 , and anti-MAPK did not label any neuronal cells in either Tg or non-Tg mice (Figure 3, p to r). These findings suggested that activated GSK-3 and Cdk5 were major kinases for phosphorylation of accumulated tau in this Tg mouse.

Gallyas-Braak Staining

To detect the formation of neurofibrillary tangles, Gallyas-Braak staining was performed. This staining labeled occasional cell bodies and the processes of the pyramidal

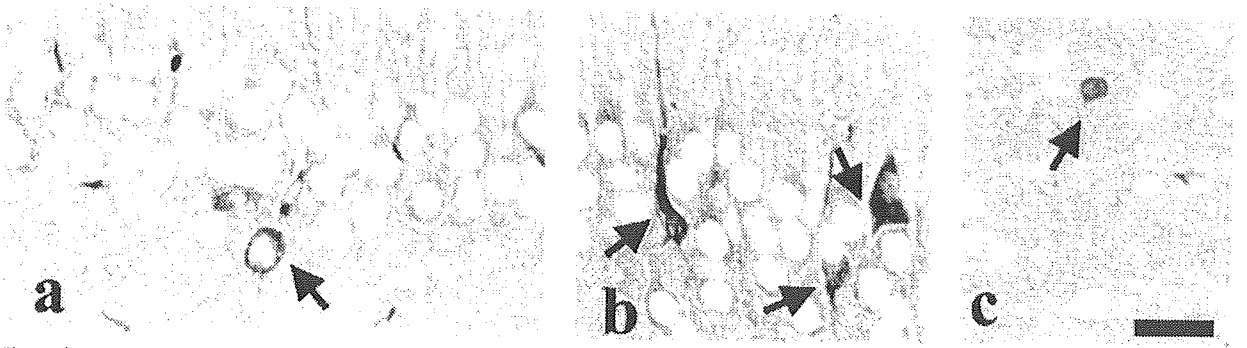

Figure 4. Gallyas-Braak staining. In 14-month-old Tau tauR406W 21807 mice, some granular cells of the hippocampus (**a** and **b**, **arrow** →) and neurons in the amygdala (**c**, →) are labeled by Gallyas-Braak staining. **Bar**, 20 m.

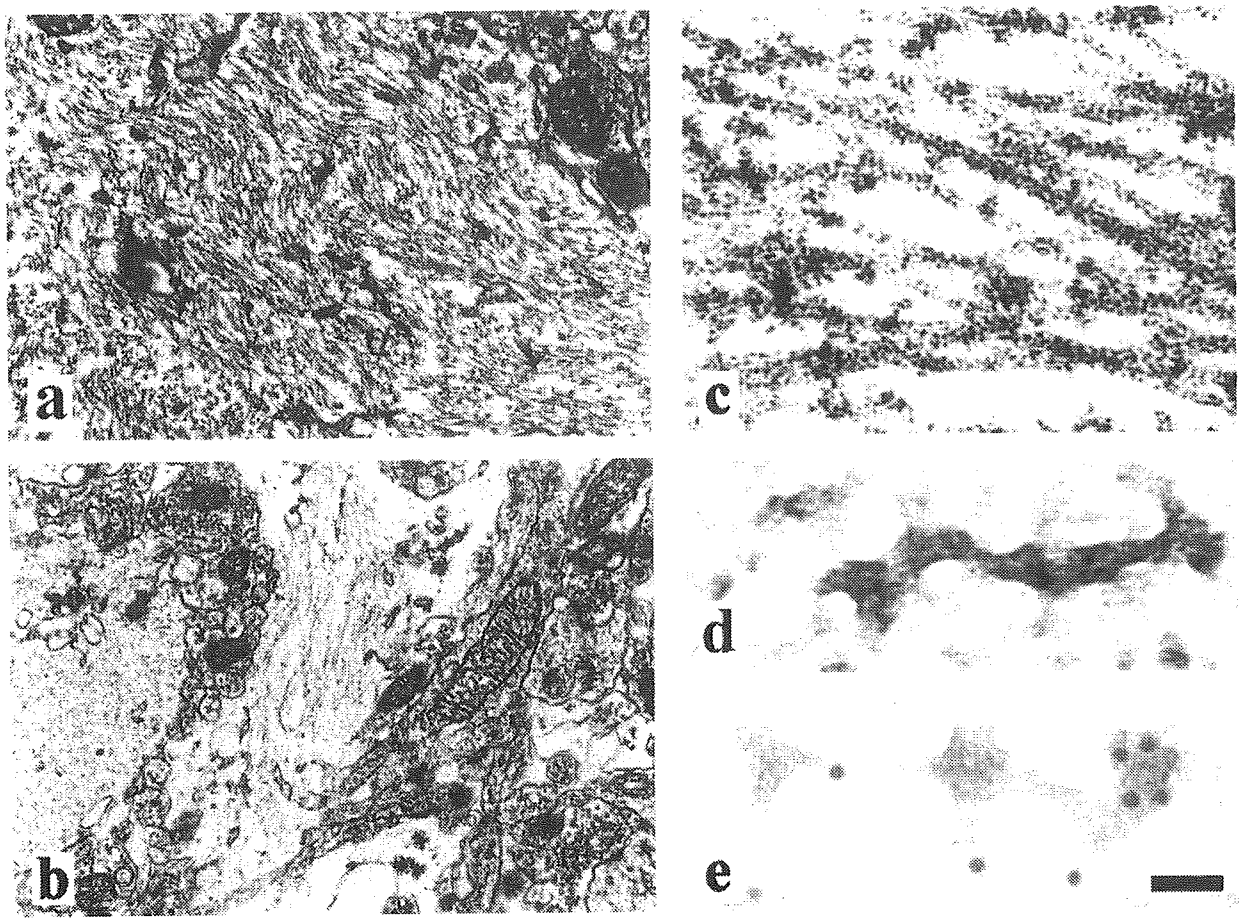

Figure 5. Electron microscopic study. Numerous filamentous aggregates are detected in the cell bodies near the nucleus of neurons in the piriform cortex (**a**, 27,000). Other filamentous aggregates were observed near the nucleus of neurons in the amygdala (**b**, 11,900). At higher magnification (**c**, 93,000), and following negative staining of sarcosyl-insoluble fractions (**d**, 130,000), 15- to 30-nm straight filaments are observed. Immunogold staining using anti-tau154 confirmed that these were aggregated tau filaments in the sarcosyl-insoluble fraction (**e**, 130,000). **Bar**, 330 nm (**a**), 750 nm (**b**), 97 nm (**c**), and 69 nm (**d** and **e**).

cells of the hippocampus (Figure 4, a and b, arrow) and amygdala (Figure 4c, arrow) in 14-month-old Tg mice.

Electron Microscopic Study

EM studies of the piriform cortex revealed massive filaments in the cell bodies of neurons (Figure 5a). Other aggregates were observed near the nucleus of neurons in the amygdala (Figure 5b). At higher magnifications, these filaments were straight and their diameters were 15 to 30 nm (Figure 5c). These filaments were present in the sarcosyl-insoluble fraction by negative staining (Figure 5d). By immunogold EM, these filaments were labeled by the anti-tau154 antibody (Figure 5e), suggesting that they consisted of accumulated human tau R406W.

Analyses of RT-PCR Transcripts and Western Blot

RT-PCR showed that expression of human *tau* mRNA transcripts (exon 9–11) was detected only in Tg mice brains, but not in non-Tg mice brains, and revealed that the level of transcription was equivalent at 6 months and 10 months of age (Figure 6a, upper panel). The expression of mouse *tau* mRNA transcripts was detected in both Tg mice brains and non-Tg mice brains (Figure 6a, lower panel). Semi-quantification of RT-PCR showed that the expression level of human *tau* R406W mRNA transcript was 119% at 6 months old and 121% at 10 months old compared to the levels of endogenous mouse *tau*.

Tris-saline (TS)-soluble human tau distributed in all neocortical regions, the hippocampus, caudate putamen, and thalamus, in addition to the brainstem-spinal cord in 5-month-old Tg mice (Figure 6b). In the TS-soluble fraction, the level of total tau protein detected by antibody tau-C was 1.8 times higher than age-matched non-Tg control mice, suggesting that the expression level of human tau R406W was about 80% that of endogenous mouse total tau protein (Figure 6c, upper panel). The Western blot findings by AT8 showed tau in the TS-soluble fractions of Tg mice was phosphorylated (Figure 6c, lower panel). Accumulated tau R406W was recognized in sarcosyl-insoluble fractions and corresponded to the highest 67-kd band of recombinant human tau 6 isoforms [33,34] (Figure 6d). The accumulation of TS-soluble or sarcosyl-insoluble tau was not observed in non-Tg

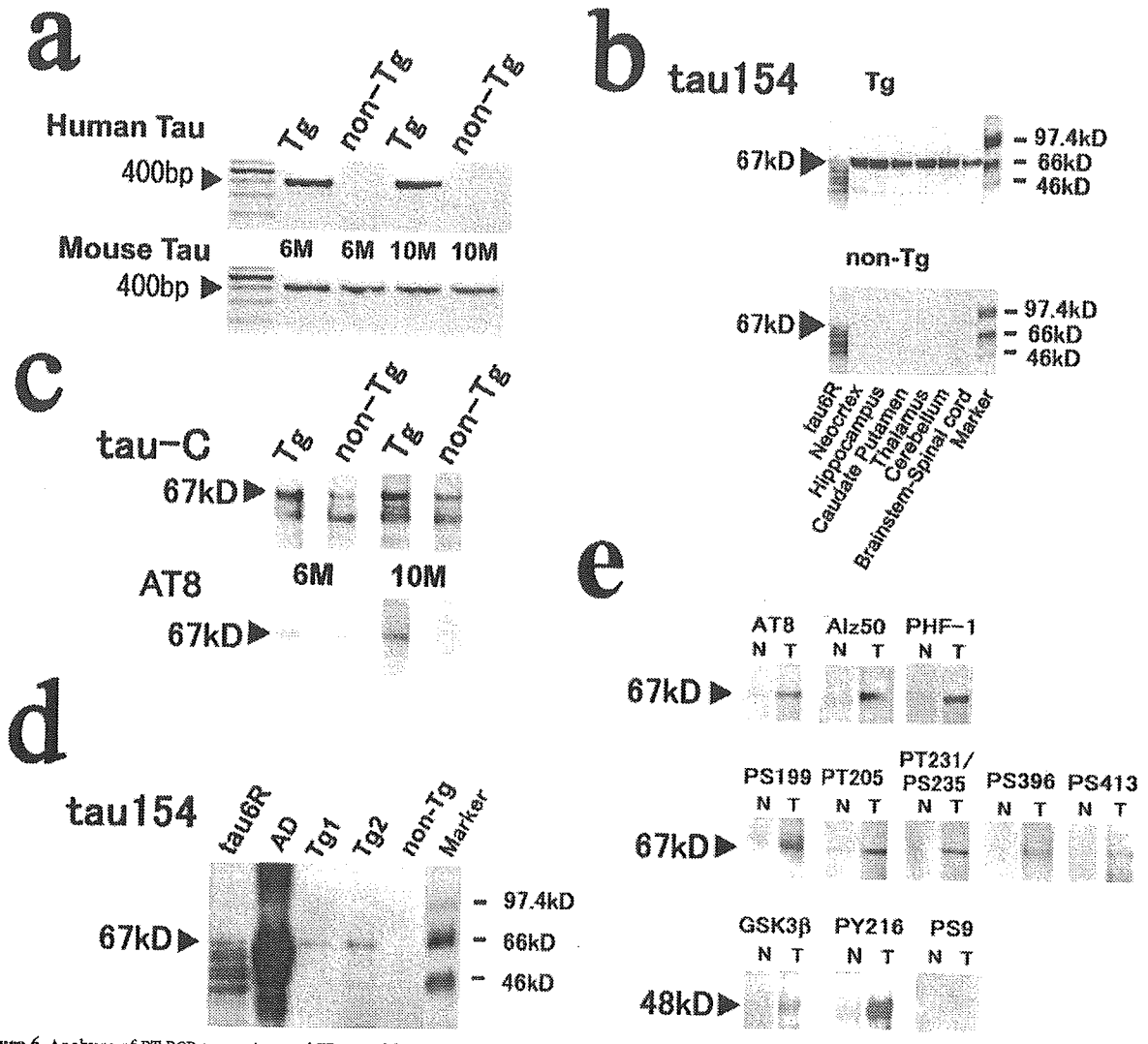

Figure 6. Analyses of RT-PCR transcripts and Western blot. Human tau mRNA transcripts (exon 9–11) were detected as 390 bp only in Tg mice brains, but not in non-Tg mice brains, and the intensity of PCR products was at the same level as 6- and 10-month-old Tg mice brains (**a, upper panel**). Mouse tau mRNA transcripts were detected in both Tg and non-Tg mice brains at the same level at 6 and 10 months of age. The signal intensities of the bands of the human tau mRNA transcripts expressed more than those of mouse tau (**a, lower panel**). The expression level of human tau R406W in a TS-soluble fraction was relatively higher in cerebral cortical areas, the hippocampus, caudate putamen, thalamus and cerebellum, in addition to the brainstem-spinal cord (**b, upper panel**). The expression of TS-soluble tau is not observed in non-Tg control mice (**b, lower panel**). In the TS-soluble fraction of the brain, the expression rate of total tau protein detected by antibody tau-C is 1.8 times higher in the Tg mouse at 6 months of age compared with an age-matched non-Tg mouse (**c, upper panel**). A Western blot using AT8 showed that tau in a TS-soluble fraction of Tg mice was phosphorylated (**c, lower panel**). In two 10-month-old TgTau(R406W) brains (Tg1, 21807 and Tg2, 21783), accumulated tauR406W was recognized in the sarcosyl-insoluble fractions and corresponded to the highest 67-kd band of recombinant tau 6 isoforms. Smear tau was detected in the brain of an AD patient; however, no accumulation of sarcosyl-insoluble tau is observed in non-Tg control mice (**d**). Accumulated tau was detected by PHF-1, Alz-50, and AT8, which corresponded to the highest 67 kd band of recombinant tau 6 isoforms (**e, upper panel**). Several phosphorylated tau antibodies showed a 67-kd band corresponding to the longest tau isoform, and accumulated tau was phosphorylated at several sites of human tau (PS199, PT205, PT231/PS235, PS396, PS413) (**e, middle panel**). GSK-3 , especially activated GSK-3 (PY216), showed high accumulation to 48kD in Tg mice brains. On the contrary, PS9, an inactivated GSK-3 antibody, did not show any bands (**e, lower panel**).

control mice (Figure 6, b to d). The Western blot with AT8, Alz-50, and PHF-1 showed a band at 67 kd in the sarcosyl-insoluble fractions of Tg mice brains (Figure 6e, upper panel). Accumulated tau was phosphorylated at serine 199, threonine 205, serine 202/threonine 205, threonine 231/serine 235, serine 396, and serine 413 in Tg mice brains (Figure 6e, middle panel). The anti-GSK-3 antibody and anti-PY216 showed a 48-kd size band. Anti-PS9 did not show any bands (Figure 6e, lower panel).

Rotarod and Step-Through Passive Avoidance Tests

There was no significant difference in rotarod test between 5-month-old Tg and non-Tg mice. The rotarod test revealed a significant decrease in retention time on the rotating rod in 10-month-old (P 0.0001) and 12-month-old Tg mice (P 0.0001) compared with their age-

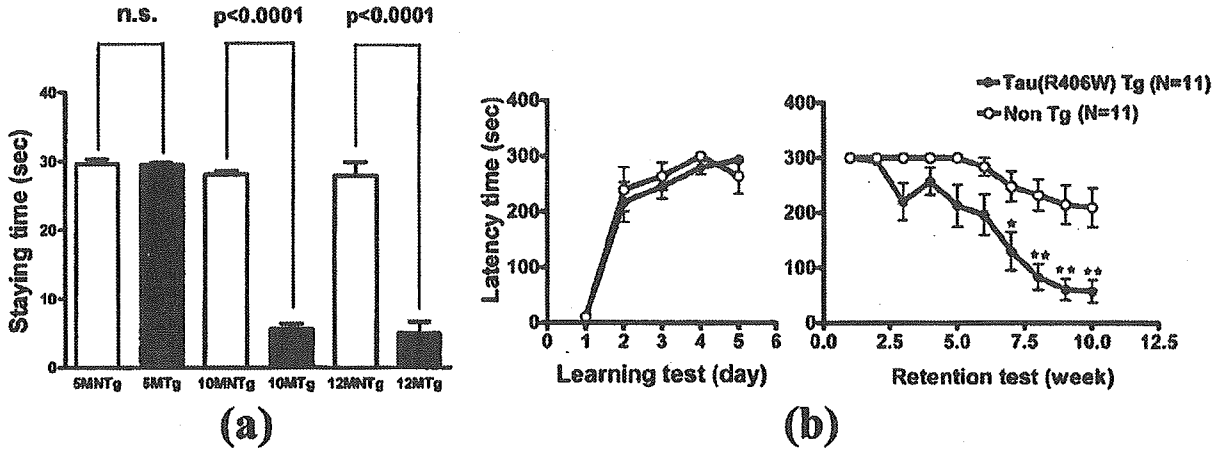

Figure 7. Behavioral examination. **a:** Rotarod test. There was no significant difference in rotarod test between 5-month-old Tg and non-Tg mice. The retention time of Tg mice (n 11) and non-Tg mice (n 11) on a rotoring rod is significantly decreased in Tg mice at 10 and 12 months of age compared with non-Tg mice (P 0.0001). **b:** Step-through passive avoidance test. Learning stages of Tg mice (**closed circle**) and non-Tg mice (**open circle**) at 10 months of age were not significantly different for 5 days (**left**). The latency time of Tg mice became shorter than that of non-Tg mice from 2.5 weeks and a significant decrease was shown from 7 weeks (P 0.05) and from 8 to 10 weeks (P 0.001) by two-way repeated measure analysis of variance.

matched non-Tg mice littermates. However, there was no significant difference in performance between 10- and 12-month-old Tg mice (Figure 7a).

The step-through passive avoidance test at 10 months of age revealed that both the Tg and non-Tg control mice learned to avoid electrical stimuli in the dark compartment within five serial trials in 1 week, with no significant difference during the learning phase. However, the retention time for the avoidance reaction in the Tg mice began to decrease 7 weeks later. This behavioral disturbance continued to worsen during the subsequent eighth, ninth, and tenth weeks compared with non-Tg control mice (P 0.0001) (Figure 7b).

Discussion

Several groups have reported wild-type tau Tg mice[35–39] and mutant-type tau Tg mice.[40–44] Tg mice expressing the wild-type of four-repeat human tau have exhibited somatodendritic localization and hyperphosphorylation of tau,[35] and prominent axonal tau accumulation in the brain and spinal cord. The shortest human three-repeat tau showed age-dependent emergence, and progression of tauopathy with Congophilic or Gallyas-Braak stain-positive, NFT-like intraneuronal inclusions in the brainstem and spinal cord.[36,37] Tau P301L Tg mice exhibited neurofibrillary tangles and neuronal loss in the anterior horn of the spinal cord.[40,41] Tau V337M Tg mice were reported to form phosphorylated and ubiquitinated tau aggregations labeled by Congo red.[42] Tau P301S Tg mice also showed neuronal loss in the spinal cord, presenting with abundant filaments consisting of hyperphosphorylated tau protein.[43] Tau R406W Tg mice under a CaMKII promoter showed Congophilic and argyrophilic tau inclusion in hippocampal neurons, and impaired associative memory during cued and contexual tests.[44]

Compared with these mice, TgTauR406W mice showed a unique distribution of tau accumulation initiating from neuronal processes to the cell bodies of neurons in the hippocampus, amygdala, and neocortices, which was accompanied by astrocytosis and microgliosis. The accumulated tau was ubiquitinated and was phosphorylated at serine 199, serine 202, threonine 205, threonine 231/serine 235, serine 396, and serine 413. These sites are also phosphorylated in Alzheimer's disease.[45] In FTDP-17 patients with *tau* R406W, the accumulated tau is phosphorylated at serine 202, threonine 205, 231, and threonine 396.[10–12] Recently, in immortalized mouse cortical cells that express low levels of endogenous tau and which were stably transfected with human tau R406W or wild-type human tau, the tau R406W was more highly phosphorylated at numerous epitopes, and showed decreased microtubule binding compared to wild-type human tau.[46] The accumulated tau R406W in our Tg mouse model therefore has phosphorylated sites in common with those observed in FTDP-17[9–13] and Alzheimer's disease.[23,47]

The expression level of tau R406W was about 80% that of the endogenous mouse tau levels by Western blot analysis. The human tau was expressed at relatively similar levels in all neocortical regions of the mice brains. Human tau R406W was clearly detected in the sarcosyl-insoluble fraction in Tg mice brains. Phosphorylated tau observed by immunostaining was revealed to accumulate in sarcosyl-insoluble fractions by Western blot.

The antibody to activated GSK-3 (PY216) detected prominent activated GSK-3 in TgTauR406W mice brains by immunocytochemistry. These findings were in agreement with similar results from Western blot analysis of the sarcosyl-insoluble fraction, indicating the close biochemical relationship between tau accumulation and the activity of GSK-3 in Tg mice brains, which is likely to occur in the brains of FTDP-17 patients with *tau* R406W[9–13] and tauopathies including AD.[23,47]

EM analysis showed straight 15- to 30-nm filaments in the cell bodies of neurons composed of expressed human mutant *tau* R406W. FTDP-17 patients with *tau*

R406W showed both paired helical filaments (with a maximum diameter of 20 to 24 nm and with periodic constrictions at 70- to 80-nm intervals) and a few straight filaments of about 12-nm diameter.[9] These filaments were located in sarcosyl-insoluble fractions.[10] In the AD brain, paired helical filaments with a diameter of 8 to 20 nm and straight filaments were also typically recovered from the sarcosyl-insoluble fraction. However, although the distribution and characteristics of the accumulated tau in TgTauR406W mice brains resembled those in Dutch patients with the same FTDP-17 (*tau* R406W) (Dutch 4 family),[10] we did not observe PHFs, but rather straight filaments, in Tg mice brains. It is conceivable that this may have arisen because our mutant transgene expressed only a single isoforms of tau. It will be necessary to undertake additional studies with transgenes allowing alternative splicing of exons 2, 3, and 10 to determine whether accumulation of all six isoforms of *tau* R406W can cause the typical PHF as seen in AD patients.

A prominent pathological findings in the brains of patients with the *Tau*R406W mutation has been reactive astrocytosis and microgliosis.[9–11] We observed prominent astrocytosis in the neocortex, amygdala, and hippocampus. Interestingly, these reactive astrocytes expressed endogenous murine tau in their cell bodies. These findings suggest that accumulated mutant human tau induced reactive astrocytosis and microgliosis, and may then exacerbate the tauopathy by further modulating the metabolism of endogenous tau. Recent studies reported the appearance of filamentous tau in oligodendrocytes and astrocytes in JNPL3 lines expressing mutant tau P301L using a murine prion promoter.[46]

In addition to pathological and biochemical findings, TgTauR406W mice demonstrated aberrant behavior. The decreased retention time in the rotarod test was due to a slow movement or a slow response causing postural instability on the rotating rod. The slow response, slow movement, and paucity of mobility resemble the parkinsonian motor deficits observed in some FTDP-17 patients, and suggests that tau accumulation in subcortical areas, especially the caudate and putamen in Tg mice brains, may cause these behavioral abnormalities. A motor deficit detected by the rotarod test started from at least 10 months and was also detected at 12 months of age (P 0.005). In the passive avoidance test, TgTauR406W mice failed to remember the noxious stimulus and moved actively from the light compartment into the dark compartment. This selective loss of acquired memory in TgTauR406W mice may have been caused by massive accumulation of phosphorylated, conformationally changed, and insoluble aggregated tau in neurons and their processes.

Taken together, all these findings indicate that the present animal model reproduced many of the principal neuropathological, biochemical, and behavioral features of FTDP-17 with the *tau* R406W mutation, not achieved by expressing tagged tau,[44] indicating the first convincing R406W tau mouse model. As a result, these TgTauR406W mice may be useful for investigating the pathogenesis of not only FTDP-17, but also other tauopathies including Alzheimer's disease,[49,50] and for developing possible therapeutic agents.

Acknowledgments

We thank Dr. M. Morishima-Kawashima and Dr. Y. Ihara for technical advice, Dr. P. Davies and Dr. D. Dickson for provision of antibodies, and Dr. M. Goedert and Dr. T. Bird for valuable discussions.

References

1. Foster NL, Wilhelmsen K, Sima AA, Jones MZ, D'Amato CJ, Gilman S: Frontotemporal dementia and parkinsonism linked to chromosome 17: a consensus conference. Ann Neurol 1997, 41:706–715
2. Poorkaj P, Bird TD, Wijsman E, Nemens E, Garruto RM, Anderson L, Andreadis A, Wiederholt WC, Raskind M, Schellenberg GD: Tau is a candidate gene for chromosome 17 frontotemporal dementia. Ann Neurol 1998, 43:815–825
3. Hutton M, Lendon CL, Rizzu P, Baker M, Froelich S, Houlden H, Pickering-Brown S, Chakraverty S, Isaacs A, Grover A, Hackett J, Adamson J, Lincoln S, Dickson D, Davies P, Petersen RC, Stevens M, de Graaff E, Wauters E, van Baren J, Hillebrand M, Joosse M, Kwon JM, Nowotny P, Heutink P, et al: Association of missense and 5 -splice-site mutations in tau with the inherited dementia FTDP-17. Nature 1998, 393:702–705
4. Spillantini MG, Murrell JR, Goedert M, Farlow MR, Klug A, Ghetti B: Mutation in the tau gene in familial multiple system tauopathy with presenile dementia. Proc Natl Acad Sci USA 1998, 95:7737–7741
5. Reed LA, Wszolek ZK, Hutton M: Phenotypic correlations in FTDP-17. Neurobiol Aging 2001, 22:89–107
6. Hasegawa M, Smith MJ, Goedert M: Tau proteins with FTDP-17 mutations have a reduced ability to promote microtubule assembly. FEBS Lett 1998, 437:207–210
7. Spillantini MG, Goedert M, Crowther RA, Murrell JR, Farlow MR, Ghetti B: Familial multiple system tauopathy with presenile dementia: a disease with abundant neuronal and glial tau filaments. Proc Natl Acad Sci USA 1997, 94:4113–4118
8. Spillantini MG, Goedert M: Tau protein pathology in neurodegenerative diseases. Trends Neurosci 1998, 21:428–433
9. Reed LA, Grabowski TJ, Schmidt ML, Morris JC, Goate A, Solodkin A, Van Hoesen GW, Schelper RL, Talbot CJ, Wragg MA, Trojanowski JQ: Autosomal dominant dementia with widespread neurofibrillary tangles. Ann Neurol 1997, 42:564–572
10. van Swieten JC, Stevens M, Rosso SM, Rizzu P, Joosse M, de Koning I, Kamphorst W, Ravid R, Spillantini MG, Niermeijer MF, Heutink P: Phenotypic variation in hereditary frontotemporal dementia with tau mutations. Ann Neurol 1999, 46:617–626
11. Saito Y, Geyer A, Sasaki R, Kuzuhara S, Nanba E, Miyasaka T, Suzuki K, Murayama S: Early-onset, rapidly progressive familial tauopathy with R406W mutation. Neurology 2002, 58:811–813
12. Matsumura N, Yamazaki T, Ihara Y: Stable expression in Chinese hamster ovary cells of mutated tau genes causing frontotemporal dementia and parkinsonism linked to chromosome 17 (FTDP-17). Am J Pathol 1999, 154:1649–1656
13. Miyasaka T, Morishima-Kawashima M, Ravid R, Heutink P, van Swieten JC, Nagashima K, Ihara Y: Molecular analysis of mutant and wild-type tau deposited in the brain affected by the FTDP-17 R406W mutation. Am J Pathol 2001, 158:373–379
14. Kozak M: Compilation and analysis of sequences upstream from the translational start site in eukaryotic mRNAs. Nucleic Acids Res 1984, 12:857–872
15. Kozak M: An analysis of vertebrate mRNA sequences: intimations of translational control. J Cell Biol 1991, 115:887–903
16. Scott MR, Kohler R, Foster D, Prusiner SB: Chimeric prion protein expression in cultured cells and transgenic mice. Protein Sci 1992, 1:986–997
17. Citron M, Westaway D, Xia W, Carlson G, Diehl T, Levesque G, Johnson-Wood K, Lee M, Seubert P, Davis A, Kholodenko D, Motter R, Sherrington R, Perry B, Yao H, Strome R, Lieberburg I, Rommens

J, Kim S, Schenk D, Fraser P, St. George Hyslop P, Selkoe DJ: Mutant presenilins of Alzheimer's disease increase production of 42-residue amyloid beta-protein in both transfected cells and transgenic mice. Nat Med 1997, 3:67–72
18. Chishti MA, Yang DS, Janus C, Phinney AL, Horne P, Pearson J, Strome R, Zuker N, Loukides J, French J, Turner S, Lozza G, Grilli M, Kunicki S, Morissette C, Paquette J, Gervais F, Bergeron C, Fraser PE, Carlson GA, George-Hyslop PS, Westaway D: Early-onset amyloid deposition and cognitive deficits in transgenic mice expressing a double mutant form of amyloid precursor protein 695. J Biol Chem 2001, 276:21562–21570
19. Duff K, Knight H, Refolo LM, Sanders S, Yu X, Picciano M, Malester B, Hutton M, Adamson J, Goedert M, Burki K, Davies P: Characterization of pathology in transgenic mice overexpressing human genomic and cDNA tau transgenes. Neurobiol Dis 2000, 7:87–98
20. Elliott JL: Cytokine upregulation in a murine model of familial amyotrophic lateral sclerosis. Brain Res Mol Brain Res 2001, 95:172–178
21. Crowe A, Ksiezak-Reding H, Liu WK, Dickson DW, Yen SH: The N terminal region of human tau is present in Alzheimer's disease protein A68 and is incorporated into paired helical filaments. Am J Pathol 1991, 139:1463–1470
22. Greenberg SG, Davies P, Schein JD, Binder LI: Hydrofluoric acid-treated tau PHF proteins display the same biochemical properties as normal tau. J Biol Chem 1992, 267:564–569
23. Yamaguchi H, Ishiguro K, Uchida T, Takashima A, Lemere CA, Imahori K: Preferential labeling of Alzheimer's neurofibrillary tangles with antisera for tau protein kinase (TPK) I/glycogen synthase kinase-3 and cyclin-dependent kinase 5, a component of TPK II. Acta Neuropathol (Berl) 1996, 92:232–241
24. Wolozin BL, Pruchnicki A, Dickson DW, Davies P: A neuronal antigen in the brains of Alzheimer patients. Science 1986, 232:648–650
25. Tomidokoro Y, Ishiguro K, Harigaya Y, Matsubara E, Ikeda M, Park J-M, Yasutake K, Kawarabayashi T, Okamoto K, Shoji M: A amyloidosis induces the initial stage of tau accumulation in APPsw mice. Neurosci Lett 2001, 299:169–172
26. Ishiguro K, Sato K, Takamatsu M, Park J, Uchida T, Imahori K: Analysis of phosphorylation of tau with antibodies specific for phosphorylation sites. Neurosci Lett 1995, 202:81–84
27. Jicha GA, Berenfeld B, Davies P: Sequence requirements for formation of conformational variants of tau similar to those found in Alzheimer's disease. J Neurosci Res 1999, 55:713–723
28. Goedert M, Jakes R, Vanmechelen E: Monoclonal antibody AT8 recognises tau protein phosphorylated at both serine 202 and threonine 205. Neurosci Lett 1995, 189:167–169
29. Planel E, Yasutake K, Fujita SC, Ishiguro K: Inhibition of protein phosphatase 2A overrides tau protein kinase I/glycogen synthase kinase 3 beta and cyclin-dependent kinase 5 inhibition and results in tau hyperphosphorylation in the hippocampus of starved mouse. J Biol Chem 2001, 276:34298–34306
30. Paxinos G, Franklin KB: The Mouse Brain in Stereotaxic Coordinates, ed 2. Edited by Paxinos G, Franklin KB. San Diego, Academic Press, 2001
31. Ikarashi Y, Kuribara H, Shiobara T, Takahashi A, Ishimaru H, Maruyama Y: Learning and memory in mice treated with choline oxidase, a hydrolytic enzyme for choline. Pharmacol Biochem Behav 2000, 65:519–522
32. Ikarashi Y, Harigaya Y, Tomidokoro Y, Kanai M, Ikeda M, Matsubara E, Kawarabayashi T, Kuribara H, Younkin SG, Maruyama Y, Shoji M: Decreased level of brain acetylcholine and memory disturbance in APPsw mice. Neurobiol Aging 2004, 25:483–490
33. Goedert M, Spillantini MG, Cairns NJ, Crowther RA: Tau proteins of Alzheimer paired helical filaments: abnormal phosphorylation of all six brain isoforms. Neuron 1992, 8:159–168
34. Goedert M, Jakes R: Expression of separate isoforms of human tau protein: correlation of the tau pattern in brain and effects on tubulin polymerazation. EMBO J 1990, 9:4225–4230
35. Gotz J, Probst A, Spillantini MG, Schafer T, Jakes R, Burki K, Goedert M: Somatodendritic localization and hyperphosphorylation of tau protein in transgenic mice expressing the longest human brain tau isoform. EMBO J 1995, 14:1304–1313
36. Ishihara T, Hong M, Zhang B, Nakagawa Y, Lee MK, Trojanowski JQ, Lee VM: Age-dependent emergence and progression of a tauopathy in transgenic mice overexpressing the shortest human tau isoform. Neuron 1999, 24:751–762
37. Ishihara T, Zhang B, Higuchi M, Yoshiyama Y, Trojanowski JQ, Lee VM: Age-dependent induction of congophilic neurofibrillary tau inclusions in tau transgenic mic. Am J Pathol 2001, 158:555–562
38. Spittaels K, Van den Haute C, Van Dorpe J, Bruynseels K, Vandezande K, Laenen I, Geerts H, Mercken M, Sciot R, Van Lommel A, Loos R, Van Leuven F: Prominent axonopathy in the brain and spinal cord of transgenic mice overexpressing four-repeat human tau protein. Am J Pathol 1999, 155:2153–2165
39. Probst A, Gotz J, Wiederhold KH, Tolnay M, Mistl C, Jaton AL, Hong M, Ishihara T, Lee VM, Trojanowski JQ, Jakes R, Crowther RA, Spillantini MG, Burki K, Goedert M: Axonopathy and amyotrophy in mice transgenic for human four-repeat tau protein. Acta Neuropathol (Berl) 2000, 99:469–481
40. Lewis J, McGowan E, Rockwood J, Melrose H, Nacharaju P, Van Slegtenhorst M, Gwinn-Hardy K, Paul Murphy M, Baker M, Yu X, Duff K, Hardy J, Corral A, Lin WL, Yen SH, Dickson DW, Davies P, Hutton M: Neurofibrillary tangles, amyotrophy and progressive motor disturbance in mice expressing mutant (P301L) tau protein. Nat Genet 2000, 25:402–405
41. Gotz J, Chen F, Barmettler R, Nitsch RM: Tau filament formation in transgenic mice expressing P301L tau. J Biol Chem 2001, 276:529–534
42. Tanemura K, Murayama M, Akagi T, Hashikawa T, Tominaga T, Ichikawa M, Yamaguchi H, Takashima A: Neurodegeneration with tau accumulation in a transgenic mouse expressing V337M human tau. J Neurosci 2002, 22:133–141
43. Allen B, Ingram E, Takao M, Smith MJ, Jakes R: Abundant tau filaments and nonapoptotic neurodegeneration in transgenic mice expressing human P301S tau protein. J Neurosci 2002, 22:9340–9351
44. Tatebayashi Y, Miyasaka T, Chui DH, Akagi T, Mishima K, Iwasaki K, Fujiwara M, Tanemura K, Murayama M, Ishiguro K, Planel E, Sato S, Hashikawa T, Takashima A: Tau filament formation and associative memory deficit in aged mice expressing mutant (R406W) human tau. Proc Natl Acad Sci USA 2002, 99:13896–13901
45. Morishima-Kawashima M, Hasegawa M, Takio K, Suzuki M, Yoshida H, Titani K, Ihara Y: Proline-directed and non-proline-directed phosphorylation of PHF-tau. J Biol Chem 1995, 270:823–829
46. Krishnamurthy PK, Johnson GV: Mutant (R406W) human tau is hyperphosphorylated and does not efficiently bind microtubules in a neuronal cortical cell model. J Biol Chem 2004, 279:7893–7900
47. Ferrer I, Barrachina M, Puig B: Glycogen synthase kinase-3 is associated with neuronal and glial hyperphosphorylated tau deposits in Alzheimer's disease, Pick's disease, progressive supranuclear palsy, and corticobasal degeneration. Acta Neuropathol (Berl) 2002, 104: 583–591
48. Lin WL, Lewis J, Yen SH, Hutton M, Dickson DW: Filamentous tau in oligodendrocytes and astrocytes of transgenic mice expressing the human tau isoform with the P301L mutation. Am J Pathol 2003, 162:213–218
49. Lewis J, Dickson DW, Lin WL, Chisholm L, Corral A, Jones G, Yen SH, Sahara N, Skipper L, Yager D, Eckman C, Hardy J, Hutton M, McGowan E: Enhanced neurofibrillary degeneration in transgenic mice expressing mutant tau and APP. Science 2001, 293:1487–1491
50. Gotz J, Chen F, van Dorpe J, Nitsch RM: Formation of neurofibrillary tangles in P301L tau transgenic mice induced by Abeta 42 fibrils. Science 2001, 293:1491–1495

© Med Sci Monit, 2005; 11(5): CS23-26
PMID: 15874892

WWW.MEDSCIMONIT.COM
Case Study

Received: 2004.12.14
Accepted: 2005.02.17
Published: 2005.05.05

Probable chronic viral encephalitis with microglial nodules in the entire brain: a case report with necropsy

Authors' Contribution:
A Study Design
B Data Collection
C Statistical Analysis
D Data Interpretation
E Manuscript Preparation
F Literature Search
G Funds Collection

Toshihiro Imaizumi[1BCEF], Shinya Nishizaka[1B], Mitsuyoshi Ayabe[1BDE], Hiroshi Shoji[1ABDEFG], Takashi Ichiyama[2BD], Yasuo Sugita[3BDE]

[1] First Department (Neurology) of Internal Medicine, Kurume University School of Medicine, Kurume, Japan
[2] Department of Pediatrics, Yamaguchi University School of Medicine, Yamaguchi, Japan
[3] Department of Pathology, Saga Medical School, Saga, Japan

Source of support: This study was supported by a grant from the Cognitive and Molecular Research Institute of Brain Diseases, Kurume University, Japan

This paper was presented at the 6th Japanese Neuroinfectious Congress held in Sapporo, Japan in July of 2001

Summary

Background: Chronic encephalitis has rarely been seen, probably due to its viral origins, which may produce the disease in healthy or immunocompromised hosts. The etiology and pathophysiology of these types of encephalitis have not yet been clarified.

Case Report: A 63-year-old Japanese woman with underlying multiple myeloma developed chronic encephalitis with fever and progressive dementia, bilateral mild thalamic lesions on magnetic resonance imaging, and a prolonged pleocytosis, normal glucose value, and elevated interleukin-6 and interferon-γ in the cerebrospinal fluid (CSF). The patient died of pneumonia 6 months after the onset of illness, and diffuse microglial nodules were found in the entire brain. No causative viral agents were identified by polymerase chain reaction and serological tests.

Conclusions: The patient was presumed to have suffered from chronic viral encephalitis, based on clinical findings, including CSF and cytokine changes. Microglial nodules are observed in flavivirus group encephalitides, Rickettsia infections, and cytomegalovirus encephalitis in immunocompromised hosts. The possible pathogenesis of this rare encephalitis is discussed.

key words: **chronic viral encephalitis • microglial nodule • Japanese encephalitis • flavivirus • multiple myeloma**

Full-text PDF: http://www.MedSciMonit.com/pub/vol_11/no_5/6747.pdf

Word count: 1840
Tables: 1
Figures: 3
References: 20

Author's address: Hiroshi Shoji, MD, First Department (Neurology) of Internal Medicine, Kurume University School of Medicine, Asahi-machi 67, Kurume, 830-0011 Japan, e-mail: hshoji@med.kurume-u.ac.jp

BACKGROUND

Microglial nodules are observed in many infectious central nervous system (CNS) diseases, particularly viral encephalitis [1,2]. Among human viral encephalitides, first Japanese encephalitis (JE) is considered for the histological findings, in which numerous microglial nodules are seen in the gray matter from the cortex to the spinal cord. Other infectious CNS diseases include tick-borne encephalitis, St. Louis encephalitis, West Nile encephalitis, Pette-Doring encephalitis, and other Rickettsial infections [3–6]. Recently, microglial nodules have been described in cytomegalovirus (CMV) encephalopathy and cryptococcus meningitis in immunocompromised hosts, such as those with AIDS [7–10]. To date, subacute or chronic viral encephalitis with glial nodules are limited to several diseases (Table 1).

We here report a case of chronic viral encephalitis with underlying multiple myeloma (MM) characterized by fever, progressive dementia and decorticate posture, bilateral thalamic lesions on magnetic resonance imaging (MRI), mild pleocytosis, and elevated interleukin (IL)-6 and interferon (IFN)-γ in the cerebrospinal fluid (CSF). Six months after onset, the patient died of pneumonia, and diffuse microglial nodules were found throughout the entire brain on autopsy.

CASE REPORT

A 63-year-old Japanese woman was admitted to a hospital in Kurume with pneumonia in January, 1998. At age 52, she had been operated on for myoma, and at age 59, she had been diagnosed with pyelonephritis. She had not been overseas for the past 10 years.

After her 1998 admission, her pneumonia reocurred repeatedly. It was suspected that she was immunocompromised, and testing revealed that she had IgG-k type MM. She was given a small amount of melphalan and predonisolone. In July of 1999 she developed a fever of 39°C, and began to display such symptoms as delayed verbal response and cognitive impairment. In mid-August, disorientation and dementia-like symptoms appeared, and she was admitted to our University Hospital (Figure 1).

Upon admission, her blood pressure was 152/88 mmHg, pulse 84/min, temperature 38.2°C, and cardiac and respiratory sounds normal. She was in a confusional state. Apraxia and agnosia were not seen, deep tendon reflexes were decreased, the Babinski reflex was negative on both sides, and recto-urinary disturbances were present.

Other results were as follows: Erythrocyte sedimentation rate, 45 mm/1 hr, red blood cell count, 299×10^4; white blood cells, 4700/μL, CRP, 2.48 mg/dl; LDH, 1049 u/l; BUN, 23.1 mg/dl; creatinine, 0.7 mg/dl; Na,134 mEq/l; IgG k M protein (+); I gA, 14 mg/dl; IgM, 19 mg; and IgG 1190mg. Squamous cell carcinoma (SCC) was 2.0 ng/ml (normal <2.0 ng/dl), The serum Venereal Disease Research Laboratory (VDRL) test was negative. The serum JE virus complement fixation (CF) titer was 1: 8. Serologic tests for herpes simplex virus (HSV), varicella-zoster virus (VZV), CMV, Epstein-Barr virus (EBV), measles virus and human immunodeficiency virus (HIV) were all negative. The CSF contained 14 cells/μL (lymphocytes), 48 mg/dl protein, 68 mg/dl glucose, and 10.8 ng/ml (positive >10ng/ml) neuron specific enolase (NSE), and her 14-3-3 protein was negative. The CSF concentrations of tumor necrosis factor (TNF)-α, interleukin (IL)-2, IL-6, interferon (IFN)-γ, and IL-10 were determined using sandwich-type enzyme-linked immunosorbent assay (ELISA) kits. The cytokine measurements were: TNF-α <2.8 pg/ml (normal range <6.1), IL-2 5.1 (<4.6), IL-6 63.6 (<6.1), IFN-γ 65.6 (<6.1), and IL-10 4.3 (<6.1). A nested CSF PCR was performed using primer sequences for the DNA polymerase gene region that are common to the herpesvirus groups for HSV, VZV, CMV, EBV, and human herpesvirus 6, but the results were negative. An ECG and chest X-ray were unremarkable, and a skull X-ray revealed patchy lesions. A brain MRI exhibited mild abnormal lesions in the bilateral thalami and deep white matter (Figure 2). An electroencephalogram (EEG) showed generalized slow waves. Bone marrow testing revealed 1.6×10^4 nuclear cells (normal: $5\sim20\times10^4$) and 3.8% plasma cell. Culture tests for bacteria in the blood and CSF were negative.

Table 1. Subacute or chronic viral encephalitis presenting with glial nodule.

Japanese encephalitis
West Nile encephalitis
Russian spring-summer encephalitis
Pette-Doring encephalitis
Herpes simplex encephalitis
Cytomegalovirus encephalitis
Epstein-Barr virus encephalitis
Measles encephalitis
Unknown etiology

Clinical course: The patient had a persistent fever of 38°C and progressive dementia, and the source of the infections or MM was reexamined. CSF pleocytosis ($14\sim45/mm^3$) continued, predominantly with lymphocytes. Collagen disease, malignancy, and metabolic diseases were ruled out, based on the laboratory data. Creutzfeld-Jakob disease was suspected because of the progressive dementia, decorticate posture, myoclonus, and NSE of 10.8 ng/ml in the CSF. However, an assay for the CSF 14-3-3 protein was negative, and periodic synchronous discharge (PSD) was not seen throughout the entire course. In January of 2000, her condition was complicated by pneumonia, and the sputum PCR for the CMV-DNA was positive. Ganciclovir was initiated, but her respiratory insufficiency increased, and she died on January 31, 2000. A necropsy was performed on her brain only.

PATHOLOGICAL FINDINGS

At autopsy, the brain weighed 1340 g. Macroscopic findings revealed only slight vascular congestion and localized swelling. Histologically, there were numerous glial nodules consisting of lymphocytes and astrocytes in the entire brain (frontal, both hippocampi, the temporal and basal ganglia, and the occipital lobes) with marked gliosis (Figure 3 A–D). Slight softening was seen in the left hippocampus. Although the MRI had revealed

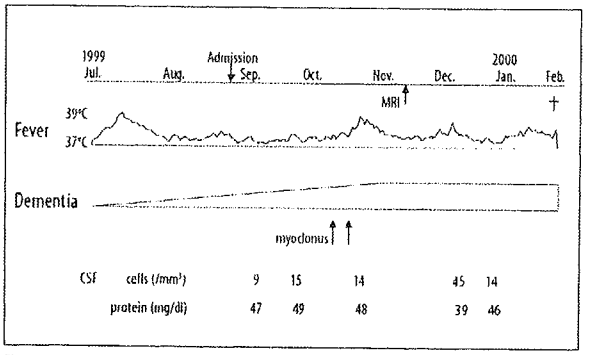

Figure 1. Clinical course. CSF – cerebrospinal fluid.

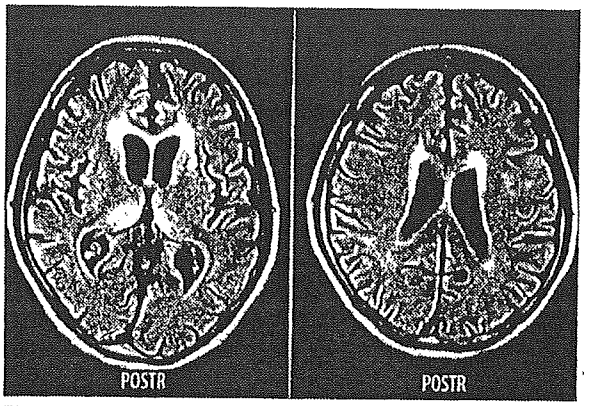

Figure 2. MRI T2WI revealed high intensity lesions in both thalami and deep white matter (arrows).

bilateral mild thalamic and subcortical lesions, the histological distribution of the microglial nodules at necropsy were not correlated with the MRI lesions. In the hemisphere, cerebellum, and brainstem, no neuronal cell loss or softening, such as is found in Creutzfeldt-Jakob disease, were observed.In addition, immunostaining for the prion protein was negative.

Serological tests

After her autopsy, the JE virus ELISA IgG and IgM, and the anti-flavivirus antibodies, were examined using two CSF samples which had been obtained one and three months after the onset of illness. However, the results were all <1:10. The serial serum JE virus antibody could not be measured, because the sera were not stored. A virus isolation test from the CSFs using VERO cells was negative.

Discussion

The present case showed fever, progressive dementia, and mild CSF lymphocytic pleocytosis and normal glucose values during the whole course of the illness, and the CSF cytokine findings, including elevated IL-6 and INF-γ, were suggestive of viral infections [11–13]. Thus, chronic viral encephalitis was diagnosed rather than acute viral encephalitis or bacterial or parasitic meningoencepalitis. The MRI taken three months after onset revealed diffuse subcortical lesions, with bilateral mild thalamic changes. The EEG exhibited diffuse slow waves. At necropsy, histologically microglial nodules and lymphocyte perivascular cuffing were found throughout the entire brain.

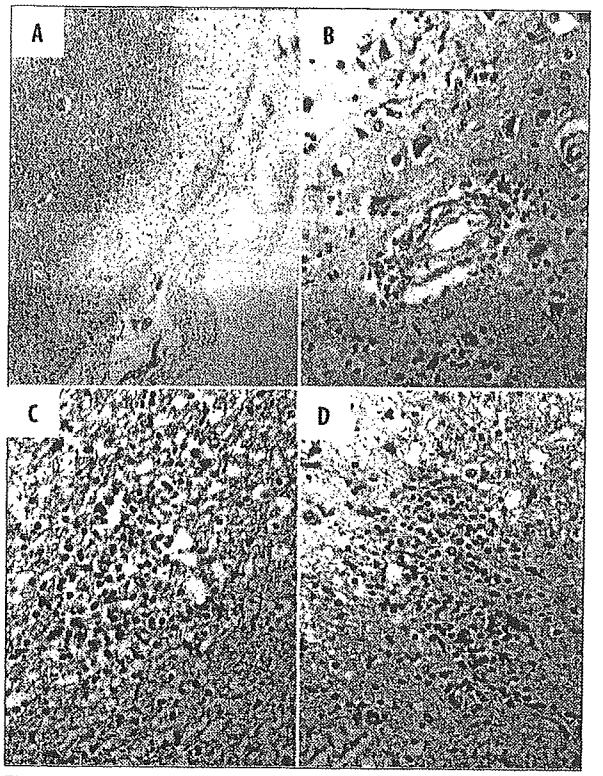

Figure 3. (**A**) 25×HE. Microscopic examination revealed cellular infiltration diffusely throughout the brain. Inflammatory cell infiltration was also noted in the leptomeniges. The cellular infiltrate consisted largely of lymphocytes. (**B**) 20×HE. A characteristic feature was the presence of perivascular cuffing. Lymphocytes had infiltrated the Virchow-Robin spaces in the small vessels. (**B–D**) 200×HE. The microglial cells were seen to form rod cells throughout the brain. (**C–D**) Microglial nodules, which consisted of a collection of lymphocytes, astrocytes, and hypertrophied microglial cells, were also seen throughout the brain.

The macrophages in the involved central nerve tissue were mostly derived hematogenously, rather than having originated from microglial cells and finally returned to the blood. Several microglial cells had gathered around and phagocyte a degenerated neuron, a process which is called neuronophagia. These microglial cells, astrocytes, or lymphocytes joined the surrounding neurons to form microglial nodules [1,2]. Such micronodules are often noted in flavivirus group encephalitides such as JE, West Nile encephalitis, and tick-borne encephalitis. They are also found in Pette-Doring encephalitis, typhus fever, and other Rickettsia infections [3–6]. In addition, microglial nodules have recently been reported in CMV encephalopathy and cryptococcus infections in immunocompromised hosts, such as those with AIDS [7–10].

At the acute to chronic stage in JE, microglial nodules, degeneration/necrosis, lymphocyte perivenous infiltration, and localized round necrosis are observed. The thalamus or substantia nigra is severely involved, and the cerebral cortex, basal ganglia, cerebellum, and brainstem are also involved [2]. Clinically, extrapyramidal signs such as tremor or rigidity are often seen with bilateral MRI lesions in the thalami and basal ganglia [14,15]. Organic person-

ality syndrome may remain as sequela [16]. A diagnosis of JE in our case could be ruled out because the chronic form of JE is rare, and the CSF ELISA IgG and IgM antibodies to the JE virus were negative, although low-serum CF antibodies to the JE virus were observed.

Pette-Doring encephalitis, which was first described in Germany in 1939, is regarded as pathologically similar to JE [2,17]: pathologically mild thalamic lesions have been found in this disease, although, unlike in JE, the basal ganglia or substantia nigra are not involved. The subacute onset, mild CSF pleocytosis, and diffuse panencephalitis closely resembled that found in our case; however, the etiology of Pette-Doring encephalitis has not been identified, and no clinical cases have been reported except in Germany.

Several tick-borne encephalitides such as Central European encephalitis (CEE) or Russian Spring-Summer encephalitis (RSSE) in Europe and the USSR have been reported, but these exhibit predominantly gray matter lesions. These tick-borne encephalitides may sometimes produce subacute or chronic encephalitic forms [3,18]. In addition, West Nile encephalitis has spread throughout the entire U.S. [19], and an outbreak might occur in Japan. However, these flavivirus group encephalitides can be differentiated based on the negativity of the anti-flavivirus antibody.

With regards to other possible encephalitides presenting with microglial nodules, typhus fever or Rickettsial diseases such as Tsutsugamushi disease could be ruled out based on the lack of characteristic skin symptoms or gastrointestinal symptoms.

In CMV encephalitis, microglial nodule ventriculitis, focal parenchymal necrosis, isolated cytomegalic cells, leptomeningitis, a change of endothelial cells, and demyelinization have been described [7,8,20]. During the course of the disease course in our patient, PCR revealed CMV-DNA in the sputum, suggesting that the patient had CMV pneumonia. In addition, the case was complicated by retinitis. However, CMV encephalitis exhibits cytomegalic inclusion bodies in the brain. Another possible cause of microglial nodules in the immunocompromised host is cryptococcus neoformans encephalopathy, in which microglial nodules are usually seen in the basal ganglia or brainstem, with multinucleate giant cells in cases of HIV encephalopathy [10].

Conclusions

The present case was characterized by chronic encephalitis with a prolonged mild pleocytosis, MRI thalamic lesions, and diffuse microglial nodules in the entire brain at necropsy. The CSF findings, including elevated IL-6 and IFN-γ, strongly suggested viral encephalitis. However, the causative virus was not identified despite intensive PCR and serological tests. Flavivirus group encephalitides, or CMV encephalitis in an immunocompromised host, were discussed as possible differential diseases. We have rarely encountered clinical cases of subacute or chronic unknown encephalitis probably with a viral origin, or similar cases which exhibited MRI or EEG abnormalities (Monzen T. unpublished data, the 9th Japanese Neuroinfectious Congress, Hirosaki, 2004.10). Our case may help to shed some light on the causes of chronic unknown viral encephalitis.

Acknowledgements

We would like to thank Dr. H Sasaki of the Kyusyu University Brain Institute for his analysis of the CSF 14-3-3 protein, Prof. T Shirabe of Kawasaki Medical College for his immunostaining of the prion protein, Prof. K Morita of Ngasaki University for his measurements of the Japanese encephalitis antibody and anti-flavivirus antibody, and Prof. K Nagashima of Hokkaido University School of Medicine for his valuable comments.

Rererences:

1. Esiri MM, Kennedy PGE: Virus diseases. In: Graham DI, Lantos PL editors, Greenfield's Neuropathology 6th ed. New York: Oxford University Press, 1997; 2: 15–41
2. Takeya S: Introduction to general neuropathology. Igakushoin, Tokyo, 1970
3. Alkadhi H, Kollias SS. MRI in tick-borne encephalitis. Neuroradiology, 2000; 42: 753–55
4. Sampson BA, Ambrosi C, Charlot A et al: The pathology of human West Nile virus infection. Hum Pathol, 2000; 31: 527–31
5. Omalu BI, Shakir AA, Wang G et al: Fatal fulminant pan-meningo-polioencephalitis due to West Nile virus. Brain Pathol, 2003; 13: 465–72
6. Solomon T, Mallewa M: Dengue and other emerging flaviviruses. J Infect, 2001; 42: 104–15
7. Setinek U, Wondrusch E, Jellinger K et al. Cytomegalovirus infection of the brain in AIDS: a clinicopathological study. Acta Neuropathol, 1995; 90: 511–15
8. Booss J, Winkler SR, Griffith BP, Kim JH: Viremia and glial nodule encephalitis after experimental systemic cytomegalovirus infection. Lab Invest, 1989; 61: 644–49
9. Grafe MR, Wiley CA: Spinal cord and peripheral nerve pathology in AIDS: the roles of cytomegalovirus and human immunodeficiency virus. Ann Neurol, 1989; 25: 561–66
10. Edelman M, Birkenhauer MC, Steinberg JJ et al: Microglial nodule encephalitis: limited CNS infection despite disseminated systemic cryptococcosis. Clin Neuropathol, 1996; 15: 30–33
11. Samuel CE: Antiviral actions of interferon. Interferon-regulated cellular proteins and their surprisingly selective antiviral activities. Virology, 1991; 183: 1–11
12. Finke D, Brinckmann UG, ter Meulen V, Liebelt UG: Gamma interferon is a major mediator of antiviral defense in experimental measles virus-induced encephalitis. J Viorl, 1995; 69: 5469–74
13. Fassbender K, Mielke O, Bertsch T et al: Interferon-γ-inducing factor (IL-18) and interferon-γ in inflammatory CNS diseases. Neurology, 1999; 53: 1104–6
14. Misra UK, Kalita J: Movement disorder in Japanese encephalitis. J Neurol 1997; 244: 299–303
15. Shoji H, Azuma K, Nishimura Y et al: Acute viral encephalitis: the recent progress. Intern Med 2002; 41: 420–28
16. Monnet FP: Behavioural disturbances following Japanese B encephalitis. Eur Psychiatry, 2003; 18: 269–73
17. Pette H, Doring G: Uber einheimische Panencephalomyelitis vom Charakter de. Encephalitis japonica. Dtsch Z N-heilk, 1939; 149: 7–12
18. Gritsun TS, Nuttall PA, Gould EA: Tick-borne flaviviruses. Adv Virus Res, 2003; 61: 317–71
19. Sejvar JJ, Haddad MB, Tierney BC et al: Neurologic manifestations and outcome of West Nile virus infection. JAMA, 2003; 290: 511–15
20. Arribas JR, Storch GA, Clifford DB, Tselis AC: Cytomegalovirus encephalitis. Ann Intern Med, 1996; 125: 577–87

ELSEVIER

Brain & Development 27 (2005) 595–597

BRAIN & DEVELOPMENT
Official Journal of the Japanese Society of Child Neurology

www.elsevier.com/locate/braindev

Case report

Serial MR imaging and ^{1}H-MR spectroscopy of unidentified bright objects in a case of neurofibromatosis type 1

Atsushi Imamura[a,*], Naoki Matsuo[a], Miho Okuda[a], Hideyuki Morita[a], Masako Iwata[a,b], Yoshihisa Yamazaki[a,c], Yukitoshi Takahashi[a,d]

[a]*Department of Pediatrics, Gifu Prefectural Gifu Hospital, 4-6-1 Noishiki, Gifu 500-8717, Japan*
[b]*Department of Pediatrics, Tajimi Municipal Hospital, Tajimi 507-8511, Japan*
[c]*Health and Medical Office, Aichi Children's Health and Medical Center, Obu 474-8710, Japan*
[d]*Department of Pediatrics, National Epilepsy Center Shizuoka Institute of Epilepsy and Neurological Disorders, Shizuoka 420-8688, Japan*

Received 28 October 2004; received in revised form 2 February 2005; accepted 21 February 2005

Abstract

Serial study using MR imaging and ^{1}H-MR spectroscopy (^{1}H-MRS) of unidentified bright objects (UBO) in a 9-year-old boy with neurofibromatosis type 1 (NF1) is described. UBO was indicated in the left globus pallidum at 3 years old, then appeared in the right globus pallidum at 5 years old along with left hemiconvulsion. These UBO gradually disappeared over several years. On ^{1}H-MRS, the ratios of *N*-acetylaspartate (NAA)/creatine and that of choline/creatine were each mildly reduced in the UBO. These ratios improved in parallel with disappearance of the UBO. In addition, elevation of the lactate/lipid peak was shown in UBO during the early stage, however, it disappeared in the latter. The longitudinal follow-up using MR image and ^{1}H-MRS was useful for metabolic evaluation of UBO in patients with NF1.

Keywords: Unidentified bright objects; Neurofibromatosis; MR image; MR spectroscopy; *N*-acetylaspartate; Choline; Lactate

1. Introduction

Neurofibromatosis type 1 (NF1), also known as von Recklinghausen disease, is a neurocutaneous syndrome. Patients with NF1 demonstrate an increased frequency of central nervous system abnormalities including gliomas of the optic pathways and brain. Unidentified bright objects (UBO), which is one type of central nervous system abnormality in NF1, have been shown as regions of T2 prolongation in characteristic brain sites in children with NF1. Globus pallidum, brainstem, thalamus, hypothalamus, cerebellum, and subcortical white matter are the most commonly involved sites of UBO [1–3]. The pathogenesis is not known but these findings are usually considered a benign process that may represent increased fluid within the myelin associated with hyperplastic or dysplastic glial proliferation [4]. We present a case of NF1 complicated by UBO in the bilateral globus pallidum. We discuss the association between the clinical course and the metabolic changes in UBO demonstrated in this patient using, serial MR imaging and ^{1}H-MR spectroscopy (^{1}H-MRS).

2. Case report

The child showed several cafe-au-lait spots of the skin, two Lisch nodules, and defect of the right temporal skull bone. Therefore, he was diagnosed as having NF1 at 3 years old. Serial MR images and MR spectroscopy of the brain was performed. MR image showed T2-prolongation in the left globus pallidum, which showed isointensity and lack of enhancement on T1-weighted image at 3 years old. Therefore, the lesion was diagnosed as UBO. He developed left hemiconvulsion at 6 years old. MR image demonstrated T2-prolongation, which was UBO, also in the right globus pallidum at this time. Electroencephalogram (EEG) showed paroxysmal sharp wave in the right occipital area, therefore, he was diagnosed as having partial epilepsy and administered carbamazepine. Seizures disappeared under this

* Corresponding author. Tel.: +81 58 246 1111; fax: +81 58 248 3805.
E-mail address: aimamura30@hotmail.com (A. Imamura).

0387-7604/$ - see front matter © 2005 Elsevier B.V. All rights reserved.
doi:10.1016/j.braindev.2005.02.008

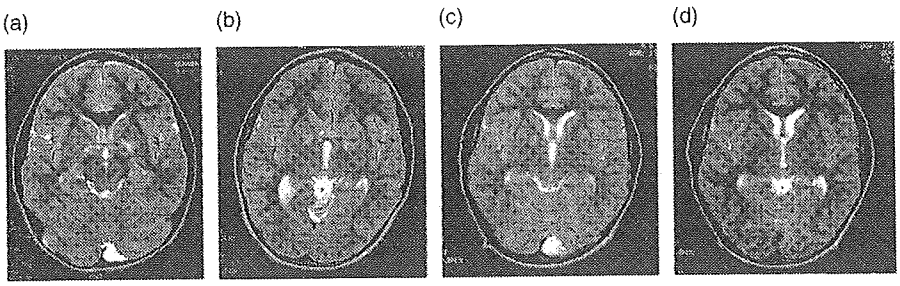

Fig. 1. Serial MRI (TR=3000 ms; TE=105 ms for T2-weighted images) of the patient, obtained at 3(a), 6(b), 8(c), and 9(d) years old, respectively. MR images demonstrated a high intensity spot (UBO) in the left globus pallidum at 3 years old, and that in the bilateral globus pallidum at 6 years old (a, b). The UBO gradually disappeared in the left globus pallidum at 8 years old, and in the right globus pallidum, at 9 years old (c, d).

treatment. MR image indicated lower T2-prolongation in the left globus pallidum at 8 years old compared to findings at than both 3 and 5 years old. Currently, the patient is nine years old, and MR imaging shows isointensity in the left globus pallidum on T2-weighted images, as well as lower T2-prolongation in the right globus pallidum (Figure 1). Serial ^{1}H-MR spectroscopy (^{1}H-MRS) was performed in this patient both at 8 and 9 years old. Localization of a $15\times 15\times 15$ mm^3 region of interest (ROI) was achieved using short TE (30 ms) point-resolved spectroscopy (PRESS) sequences. Proton MR spectra from different ROIs were acquired within measuring times of 5 min each (TR 2000 ms, 128 accumulations). ^{1}H-MRS demonstrated a low NAA/creatine (Cr) ratio in the bilateral globus pallidum (1.34 at the right, and 1.42 at the left; normal at 5–15 years, 1.80 ± 0.17) and low choline (Cho)/Cr ratio in the same region (0.60 at the right and 0.61 at the left; normal at 5–15 years, 0.89 ± 0.12) at 8 years old [5,6]. At 9 years old, the ratios of NAA/Cr and Cho/Cr in the left globus pallidum were normalized to 1.85 and 0.83, respectively, but those of NAA/Cr and Cho/Cr in the right globus pallidum remained mildly decreased at 1.66 and 0.65, respectively, (Figure 2, Table 1). A lactate/lipid peak was shown at 1.0 ppm with chemical shift on ^{1}H-MRS in the right globus pallidum at 8 years old, but this finding had disappeared at nine years old (Figure 2).

3. Discussion

Unidentified bright objects (UBO) are observed on MR imaging in 43–93% of children with neurofibromatosis type 1 (NF1) [1–4]. Clinical and pathological significance of UBO remain largely unknown, however, an association

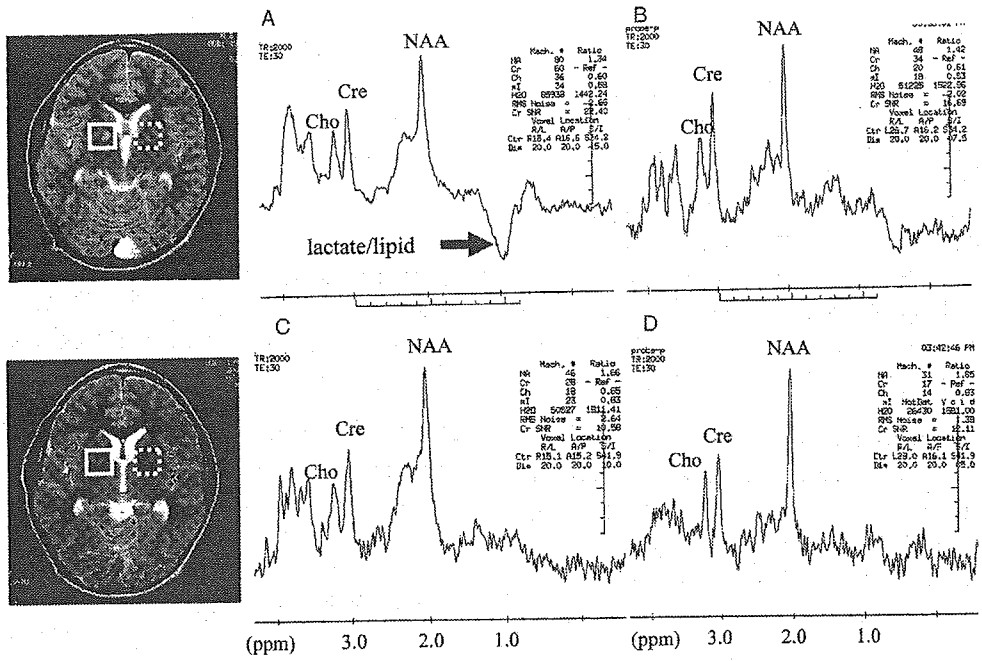

Fig. 2. Proton MR spectroscopy with short TE (30 ms) localized on the bilateral globus pallidum at 8 (upper panels) and 9 (lower panels) years old in the patient. That of the right lesion (solid square: A, C), which demonstrated T2 elongation on MRI, showed a peak of lactate/lipid at 1.0 ppm of the chemical shift at 8 years old (A), however, that on the left (dotted square: B, D), which demonstrated the disappearance of UBO, did not show a lactate/lipid peak.